AD-A091 908 HARRY DIAMOND LABS ADELPHI MD F/G 18/3
A NEAR-SURFACE BURST EMP DRIVER PACKAGE FOR NEUTRON-INDUCED SOU--ETC(U)
SEP 80 W T WYATT
UNCLASSIFIED HDL-TR-1930 NL

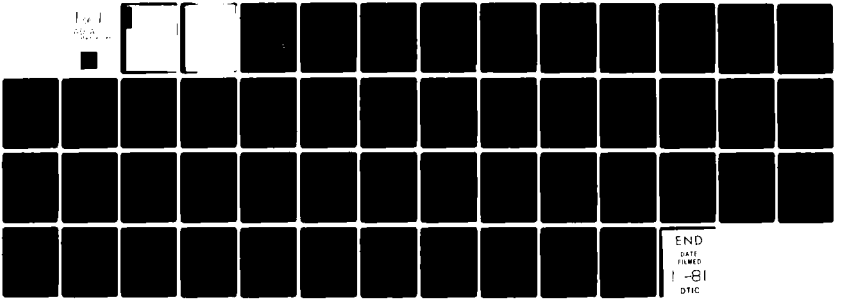

END
DATE FILMED
1-81
DTIC

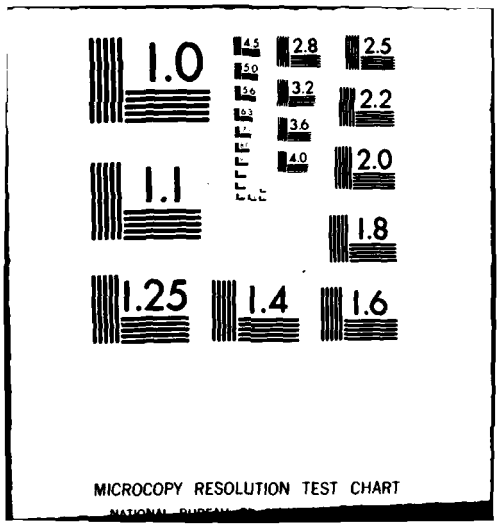
1.0
1.1
1.25
1.4
1.6
1.8
2.0
2.2
2.5
2.8
3.2
3.6
4.0
4.5
5.0
5.6
6.3
MICROCOPY RESOLUTION TEST CHART

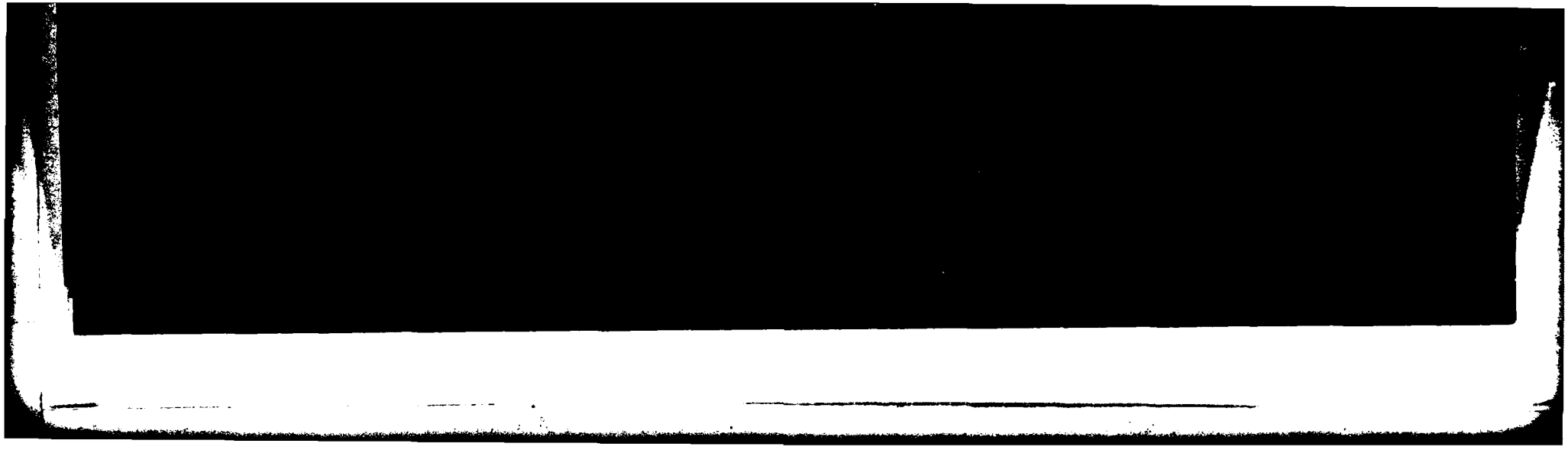

UNCLASSIFIED

SECURITY CLASSIFICATION OF THIS PAGE (When Data Entered)

REPORT DOCUMENTATION PAGE	READ INSTRUCTIONS BEFORE COMPLETING FORM
1. REPORT NUMBER: HDL-TR-1936 (14)	2. GOVT ACCESSION NO.: AD-A091 908
3. RECIPIENT'S CATALOG NUMBER: (9)	
4. TITLE (and Subtitle): A Near-Surface Burst EMP Driver Package for Neutron-Induced Sources (6)	5. TYPE OF REPORT & PERIOD COVERED: Technical Report
6. PERFORMING ORG. REPORT NUMBER	
7. AUTHOR(s): William T. Wyatt, Jr (10)	8. CONTRACT OR GRANT NUMBER(s)
9. PERFORMING ORGANIZATION NAME AND ADDRESS: Harry Diamond Laboratories, 2800 Powder Mill Road, Adelphi, MD 20783	10. PROGRAM ELEMENT, PROJECT, TASK AREA & WORK UNIT NUMBERS: Prog. El.: 6.21.20.A
11. CONTROLLING OFFICE NAME AND ADDRESS: U.S. Army Materiel Development and Readiness Command, Alexandria, VA 22333 (11)	12. REPORT DATE: Sept[illegible] 1980; 13. NUMBER OF PAGES: 50
14. MONITORING AGENCY NAME & ADDRESS (if different from Controlling Office) (12) 52	15. SECURITY CLASS. (of this report): UNCLASSIFIED; 15a. DECLASSIFICATION/DOWNGRADING SCHEDULE

16. DISTRIBUTION STATEMENT (of this Report)

Approved for public release; distribution unlimited.

17. DISTRIBUTION STATEMENT (of the abstract entered in Block 20, if different from Report)

DTIC ELECTE NOV 21 1980 S C

18. SUPPLEMENTARY NOTES

HDL Project: X759E6
DRCMS Code: 612120.H.250011
DA Project: 1L162120AH25 (16)

19. KEY WORDS (Continue on reverse side if necessary and identify by block number)

EMP	Curve fitting
Compton currents	Minimization
Ionization	Numerical integration
Nuclear explosions	Electromagnetic pulse
Radiation transport	

20. ABSTRACT (Continue on reverse side if necessary and identify by block number)

This report describes the development of a software package developed for the NEMP computer code, specifying time- and space-dependent drivers produced by neutrons emitted from a near-surface nuclear detonation in the air. Well-chosen functionals were fitted to previously obtained Monte Carlo transport results. The fit was done globally to all volume detectors and time bins together for each driver. Highly efficient minimization algorithms were employed to obtain each fit. Separate drivers for radial and

→ over

DD FORM 1 JAN 73 1473 EDITION OF 1 NOV 65 IS OBSOLETE

UNCLASSIFIED

SECURITY CLASSIFICATION OF THIS PAGE (When Data Entered)

163050

theta Compton currents and for ionization rate were determined for nine source neutron energy bands, for five classes of neutron interaction including (1) neutron direct ionization by elastic recoil and charged particle production, and secondary gamma production by (2) high energy air reactions, (3) low energy air reactions, (4) high energy ground reactions, and (5) low energy ground reactions. Burst height dependence of the drivers was determined. Comparisons with experiment and previous theory are briefly discussed. Typical driver results are presented and discussed. The package allows flexible representation of any nuclear weapon neutron energy spectrum and choice of any burst height in the near-surface regime.

CONTENTS

APPENDICES

FIGURES

CONTENTS (Cont'd)

TABLES

1. INTRODUCTION

Various Army electronic systems may be exposed to nuclear explosion effects in a tactical battlefield. Included among these nuclear effects is the nuclear electromagnetic pulse (EMP), which is a transient broadband electromagnetic field capable of damaging or upsetting electronic equipment. To predict the signature of the EMP generated by a nuclear burst, it is necessary to determine the physical parameters that induce the EMP. These parameters, called EMP drivers, are time and space varying ionization and Compton electron currents in the nuclear radiation field around the burst. Once the ionization and the currents are specified, it is usually possible to solve some form of Maxwell's equations for the EMP generated. This report summarizes the development of a software package specifying EMP drivers produced by neutrons emitted from a near-surface burst in the air. The package was designed for use with the NEMP computer code used at the Harry Diamond Laboratories (HDL). A separate report[1] summarizes the development of a similar software package for EMP drivers due to prompt gamma radiation.

2. MOTIVATION

The EMP drivers are due to one component arising from prompt gamma radiation and a second component arising from neutron radiation. The neutron component includes elastic recoil ionization (frequently called "heating") by air constituent nuclei and also includes effects of secondary gamma radiation produced by a number of neutron capture and inelastic collision reactions in the air and the ground. The development of EMP drivers by secondary gamma rays is physically similar to the development for prompt gamma radiation, although the magnitude, the direction, and the time dependence are markedly different.

Maxwell's equations for EMP from a near-surface burst are solved by the NEMP computer code.[2,3] The NEMP code requires EMP drivers to be specified in a volume extending to several kilometers from the burst point and for times extending to many milliseconds after the instant of burst. The EMP drivers must be incorporated into the code as smooth fits to results of quasi-analytic or Monte Carlo predictions. The NEMP

---

[1] *William T. Wyatt, Jr., A Near-Surface Burst EMP Driver Package for Prompt Gamma-Induced Sources, Harry Diamond Laboratories HDL-TR-1931 (1980).*

[2] *H. J. Longley, C. L. Longmire, and K. S. Smith, Development of NEMP (U), Mission Research Corp., Santa Barbara, CA, HDL-CR-75-001-1 (April 1975). (SECRET--RESTRICTED DATA)*

[3] *H. J. Longley and K. S. Smith, Developments in NEMP for 1977 (U), Mission Research Corp., Santa Barbara, CA, HDL-CR-77-0022-1 (January 1978). (SECRET--RESTRICTED DATA)*

code in many respects is an extension of the LEMP computer code[4] for EMP from surface bursts, which was initially developed from about 1966 to about 1969. The EMP drivers in the earlier LEMP code could have been modified and used in the NEMP code with certain limitations. These limitations are discussed briefly, and reasons are given for the importance of the new results reported here.

In this study, the neutron-induced EMP drivers are divided into five categories: (1) neutron elastic (recoil) ionization, (2) fast neutron air inelastic collision ($n,n'\gamma$) drivers (both Compton electron currents and ionization), (3) fast neutron ground inelastic collision ($n,n'\gamma$) and capture (n,γ) drivers, (4) thermal neutron ground capture (n,γ) drivers, and (5) thermal neutron air capture (n,γ) drivers. Of these, one would expect the NEMP geometry to introduce complications to LEMP code prescriptions for categories (1), (2), and (4), since the proximity of the ground is different. Category (5) was not treated originally by the LEMP code. Category (3) would be quite different for the NEMP code and probably of reduced magnitude. However, the cross sections for most of the above reactions have been subjected to concentrated study and revision with the advent of the Evaluated Nuclear Data File (ENDF-B, distributed Brookhaven National Laboratory, Brookhaven, NY). It is likely that new neutron transport studies based on recent ENDF-B cross sections would produce results different from those upon which the LEMP code neutron-induced EMP drivers were based. Further, by omission of the thermal neutron air capture (n,γ) drivers, the LEMP drivers were limited to times less than about 1 ms after the burst.

The LEMP authors[5] developed a newer and much more complete prescription of categories (1) through (5) based on results of Sargis and others.[6] Factors weighing against the use of these prescriptions in the NEMP code include the following: First, a newer revision (Round 3) of ENDF-B was released in 1973. Second, the only burst heights considered by Sargis were 0, 200, and 500 m, whereas the NEMP code operates principally at tactical burst heights between 0 and 200 m. Third, the new LEMP EMP driver curve fits were considered by this writer to neglect certain important ground-air interface effects such as time-dependent depletion and enhancement. Fourth, the transport results[6] were based on

---

[4] *H. J. Longley and C. L. Longmire, Development and Testing of LEMP 1, Los Alamos Scientific Laboratory, NM, LA-4346 (April 1970).*

[5] *H. J. Longley, C. L. Longmire, J. S. Malik, R. M. Hamilton, R. N. Marks, and K. S. Smith, Development and Testing of LEMP 2, A Surface Burst EMP Code (U), Mission Research Corp., Santa Barbara, CA, DNA 4097T (December 1976). (CONFIDENTIAL)*

[6] *D. A. Sargis, E. R. Parkinson, J. N. Wood, R. E. Dietz, and C. A. Stevens, Late-Time Sources for Close-In EMP, Science Applications, Inc., La Jolla, CA, DNA 3064F (August 1972).*

"energy grouped" cross sections, whereas a "point" cross-section treatment should be more accurate at deep penetrations. Fifth, a single typical source neutron energy spectrum was used in the LEMP drivers, with a parameter available for adjusting the concentration of high-energy (14-MeV) neutrons; a more desirable package would allow flexible representation of arbitrary source neutron energy spectra.

For these reasons, new Monte Carlo transport calculations have been done to describe more accurately the neutron-induced EMP drivers.[7] The extent of these calculations is summarized in table 1. Edited results of these calculations were transmitted to this writer on computer magnetic tape and used to derive the EMP driver software package reported here.

TABLE 1. MONTE CARLO DATA CHARACTERISTICS

Source neutron energy band (MeV)	Time bin boundary (s)	Burst height (m)	EMP driver
0.0 to 0.11	0.0 to 1.0(-7)*	1	Neutron direct ionization
0.11 to 0.55	1.0(-7) to 2.15(-7)	50	High-energy air, radial current
0.55 to 1.11	2.15(-7) to 4.64(-7)	100	High-energy air, theta current
1.11 to 1.83	4.64(-7) to 1.0(-6)	200	High-energy air, ionization
1.83 to 2.35	1.0(-6) to 2.15(-6)		Low-energy air, radial current
2.35 to 4.07	2.15(-6) to 4.64(-6)		Low-energy air, theta current
4.07 to 6.36	4.64(-6) to 1.0(-5)		Low-energy air, ionization
6.36 to 8.19	1.0(-5) to 2.15(-5)		High-energy ground, radial current
8.19 to 15.0	2.15(-5) to 4.64(-5)		High-energy ground, theta current
	4.64(-5) to 1.0(-4)		High-energy ground, ionization
	1.0(-4) to 2.15(-4)		Low-energy ground, radial current
	2.15(-4) to 4.64(-4)		Low-energy ground, theta current
	4.64(-4) to 1.0(-3)		Low-energy ground, ionization
	1.0(-3) to 2.15(-3)		
	2.15(-3) to 4.64(-3)		
	4.64(-3) to 1.0(-2)		
	1.0(-2) to 2.15(-2)		
	2.15(-2) to 4.64(-2)		
	4.64(-2) to 1.0(-1)		

*Read as 1.0×10^{-7}.

[7] *H. S. Schechter and M. O. Cohen, Energy Deposition Rates and Compton Electron Currents from Low-Altitude Bursts as a Function of Source Energy, Mathematical Applications Group, Inc., Elmsford, NY, HDL-CR-77-020-1 (November 1977).*

3. APPROACH

The edited results of Monte Carlo calculations contain statistical fluctuations inherent in the Monte Carlo method. The NEMP code demands smooth prescriptions of the EMP drivers to obtain useful results. One may attempt to fit smooth general functions (such as polynomials) to the Monte Carlo results by a least-squares fitting technique, for example, or one may attempt to fit the Monte Carlo results with certain appropriate smooth functional forms. By using a polynomial of sufficiently high degree, the former technique may allow the Monte Carlo results to be fitted more faithfully than the latter, but the closer fit may mean that the "noise" is being fitted instead of the underlying smooth "true answer." The same difficulty can arise by using the latter technique if too many degrees of freedom are permitted. On the other hand, if the polynomial degree is not high enough, the fit may be a poor representation of the true answer. In general, however, using appropriate smooth functional forms will involve far fewer degrees of freedom than using general functions if the functional forms are well chosen and if the fit is a global fit over the entire space-time volume of interest rather than a piecewise fit over many smaller subdivisions of the space-time volume.

The strength of the technique of using well-chosen functional forms is that physical variables usually do behave according to relatively simple physical principles that are approximately described by relatively simple functional forms. A global fit of properly chosen functional forms to Monte Carlo results could reduce the error below the statistical error of the Monte Carlo calculation. The fitting algorithm should heavily weight low-variance results over high-variance results to reduce the error.

The new edited Monte Carlo results for neutron-induced EMP drivers consist of three physical quantities (energy deposition and radial and polar components of Compton electron current) defined for 19 time intervals within 63 spatial volume detectors, for five categories of reaction (recoil, air inelastic, etc.), four burst heights, and nine source neutron energy bands (table 1). There are 646,380 quantities to be fitted. Apparently, the fitting algorithm must be highly automated to allow useful results to be obtained with a realistic investment of human effort.

4. CURVE-FITTING PROCEDURE

Thirteen distinct functions describe the time and space dependence of 13 EMP drivers:

(1) Ionization in the air from neutron elastic collisions and charged particle production (such as (n,p) and (n,α) reactions that deposit kinetic energy locally)

(2) Radial Compton electron current in the air (measured in the polar coordinate system centered at the burst) due to high-energy neutron reactions in the air (neutron energy more than 0.1 MeV)

(3) Polar Compton electron current in the air for the same as (2)

(4) Ionization in the air for the same as (2)

(5) Radial Compton electron current in the air due to low-energy neutron reactions in the air (neutron energy less than 0.1 MeV)

(6) Polar Compton electron current in the air for the same as (5)

(7) Ionization in the air for the same as (5)

(8) Radial Compton electron current in the air (measured in the polar coordinate system centered on the ground beneath the burst) due to high-energy neutron reactions in the ground

(9) Polar Compton electron current in the air for the same as (8)

(10) Ionization in the air for the same as (8)

(11) Radial Compton electron current in the air due to low-energy neutron reactions in the ground

(12) Polar Compton electron current in the air for the same as (11)

(13) Ionization in the air for the same as (11)

Drivers (2), (3), and (4) are due principally to high-energy inelastic collisions with atmospheric nitrogen. Drivers (5), (6), and (7) are due to thermal capture by atmospheric nitrogen. Drivers (8), (9), and (10) are due to inelastic collisions with the ground and fast neutron capture by the ground. Drivers (11), (12), and (13) are due to thermal neutron capture by the ground.

A mathematical notation is used to simplify the succeeding discussion. The vector functional F represents the drivers. F is dependent on time (t) and space (x,y,z). Subscript d running from 1 to 13 denotes which of the drivers is represented:

$$F_d(t,x,y,z)$$

Time t is the local time, retarded by the speed of light from the coordinate center.

The functional F_d is a functional form incorporating a certain number, n_d, of parameters p. This is written as

$$F_d(t,x,y,z;p_{di}) \quad ,$$

where p_{di}, i = 1 to n_d, is interpreted as the parameter vector of length n_d for driver d. In general, n_d is not the same for different d, but is approximately 10 in this report.

Parameters p_{di} are evidently dependent on the energy of the source neutrons producing the drivers and on the height of burst. Other variables are ignored, such as variations in water content of the air and the ground and variations in ground composition. The parameters may then be written

$$p_{di}(j,h)$$

or

$$p_{dij}(h) \quad ,$$

where j denotes the ordinal of the source neutron discrete energy band and h is the height of burst. In this way, p is a discrete function of the source neutron energy (band) and a continuous function of the height of burst. It thus appears that the EMP driver fits

$$F_d(t,x,y,z;p_{dij})$$

are defined when parameters p_{dij} are evaluated for a specific height of burst,

$$p_{dij} = p_{dij}(h) \quad .$$

The total number of functions $p_{dij}(h)$ to be determined is

$$\sum_{d=1}^{13} \sum_{i=1}^{n_d} \sum_{j=1}^{9} 1 = \sum_{d=1}^{13} \sum_{i=1}^{n_d} 9 \quad .$$

Since $n_d \sim 10$, this total is roughly 1100. Thus, there are over a thousand such functions to be specified. Determination of this many functions was a formidable undertaking and required considerable computer time (about 40 hr on an IBM System/370 Model 168).

The following strategy was adopted:

a. Through previous experience supported by trial and error, 13 functional forms were constructed to constitute driver functionals F_d. These were functions of time and space and were based on a certain number, n_d, of parameters.

b. Monte Carlo predictions for the 13 drivers were available as functions of time for each of 63 spatial volume detectors around the burst for each combination of four burst heights and nine source neutron energy bands. For a particular source neutron energy band, each driver functional was fitted to the time and space dependence of the Monte Carlo data, for each of the four sets of data corresponding to the four heights of burst (1, 50, 100, and 200 m). The fit was obtained through an optimization process by adjustment of each of the n_d parameters for the driver.

c. Four values, $\hat{p}_{dij}(h_k)$, k = 1 to 4, were thus derived for each parameter p_{dij} corresponding to the four heights of burst. These four values were approximated by simple functions of the height of burst. In some cases, a constant function was used; in other cases, a rational fraction was used. Certain constraints were imposed on the rational fraction to insure satisfactory behavior of the approximation.

d. Since parameter functions $p_{dij}(h)$ only approximated values $\hat{p}_{dij}(h_k)$, k = 1 to 4, it was desirable to readjust the amplitudes of the driver functionals $F_d(t,x,y,z;p_{dij}(h))$ to obtain a closer fit to the Monte Carlo data. Since the amplitude was by choice one of the parameters--specifically, p_{d1j}, this readjustment involved simply reoptimizing the fit to the Monte Carlo data by adjustment of this one parameter, p_{d1j}. Once this adjustment was done for each of the four heights of burst, amplitude parameter function $p_{d1j}(h)$ was refitted to these four improved values for $\hat{p}_{d1j}(h_k)$.

e. This completed the definition of all parameter functions $p_{dij}(h)$ for a particular neutron energy band, j. Process b to d was repeated for each of the nine energy bands.

This strategy was implemented through the use of two specially developed computer codes, BIGFIT and HOBFIT. BIGFIT performs a global minimization (that is, simultaneously over all volume detectors and time bins) of an error function estimating the "badness of fit" of driver functionals F_d to the Monte Carlo data. HOBFIT approximates the burst height dependence of parameter values $\hat{p}_{dij}(h_k)$ with either a constant function or a rational function. BIGFIT performs the minimization for specified parameters of the functional. In practice, the specified parameters were usually either the amplitude parameter only or all parameters of the functional.

The curve-fitting procedure is illustrated in figure 1. This procedure was performed for each source neutron energy band and each driver functional, or 9 × 13 = 117 times, except where the driver was exactly zero for an energy band. (For example, no high-energy neutron reactions can occur for a low-energy source neutron.) First, starting with trial guesses for the parameter values, BIGFIT was run four times (once for each burst height) to fit the driver functional to the Monte Carlo data for that case. All parameters were adjusted to obtain the fit. The functional parameter values so determined were stored in temporary data file FITFILE. Second, HOBFIT obtained functions approximating the burst height dependence of the parameters stored on FITFILE, saving these functions on permanent data file HOBFILE A. Third, the parameter functions were evaluated at the four burst heights, and the resulting parameter values were used as BIGFIT was rerun four times (once for each burst height) to fit the driver functional to the Monte Carlo data, this time adjusting only the amplitude parameter of the functional. The four amplitude parameter values so obtained were stored in temporary data file AMPFIT. Fourth, HOBFIT obtained a function approximating the burst height dependence of the revised amplitude parameter values on AMPFIT, saving this function on permanent data file HOBFILE B. Thus, the final amplitude parameter fits are stored on HOBFILE B, and the other parameter fits are stored on HOBFILE A.

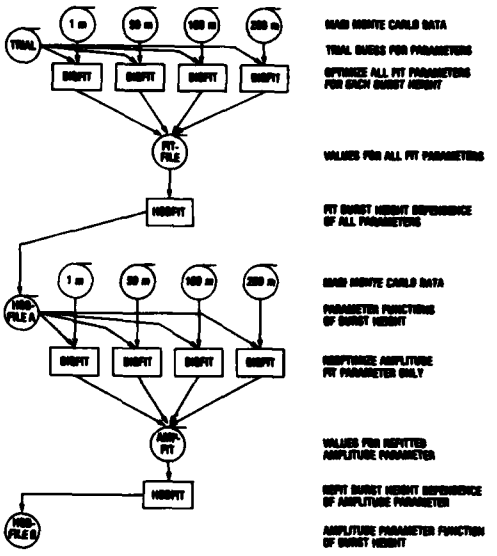

Figure 1. Fitting algorithm. Final amplitude parameter fits are created on HOBFILE B. Other parameter fits are created on HOBFILE A. This algorithm is applied to each driver for every source neutron energy band.

5. MINIMIZATION OF FIT ERROR

The goal of the curve-fitting procedure in this work is to obtain a *global* fit to the Monte Carlo data for the EMP drivers--that is, to fit a single functional to the data over the entire space-time grid of volume detectors and time bins. The global fit is desired rather than a

piecewise fit to the space or time dependence of the data. For a global fit, a penalty function is constructed that measures the suitably weighted error or the disagreement between the data and the curve fit. The curve fit is improved by reducing the magnitude of the penalty function by adjustment of the fit parameters. A best fit is obtained when the penalty function arrives at a (minimum) extremum. The penalty function is a function of the several parameters for the driver functional and, with suitable smoothness, is amenable to minimization by standard optimization algorithms.

To illustrate the curve-fitting procedure, a specific example of a driver functional is examined. Neglecting air density and mass-scaling effects for simplicity of presentation, the functional for ionization by high-energy neutron inelastic collisions in the atmosphere (that is, "air inelastic" gamma ray production) is

$$I(x,y,z,t) = p_1 ACD$$

where

x,y,z = Cartesian coordinates of the observer measured from the coordinate center on the ground beneath the burst,

t = retarded time at the point (x,y,z'),

z' = $z - h$,

h = burst height,

p_1 = amplitude parameter,

A = $1 - p_2 \exp(-zp_3)$,

C = $\exp(-tp_4)/(t^{p_5} + p_6)$,

D = $\exp(-rp_7)/(r^2 + p_8)$,

r = $\left[x^2 + y^2 + (z')^2\right]^{1/2}$.

This particular driver functional is relatively simple and incorporates range attenuation factor D, time dependence factor C, and ground depletion factor A. These factors are typical of other driver functionals, as well, although other functionals may also include time-dependent or range-dependent ground depletion (or enhancement) factors. Different time-dependence factors are used also.

In this functional, eight parameters are used so that the penalty function is a function of eight variables. The penalty function is defined as function P of parameter vector p_k, k = 1 to 8:

$$P(p_k) \equiv \sum_{i,j} \left\{ \left[f_{ij} - f(x_i, y_i, z_i, t_j; p_k) \right]^2 \frac{w_{ij}}{V_{ij}} \right\},$$

where the summation is performed over all i and j and where

i = a volume detector index running from 1 to 63,

j = a time bin index running from 1 to 19,

f_{ij} = the driver Monte Carlo score in the ith detector and jth time bin,

$f(x_i, y_i, z_i, t_j; p_k)$ = the integral, over the ith detector and jth time bin, of driver functional $F(x_i, y_i, z_i, t_j; p_k)$ (d subscript omitted from F) evaluated for parameter vector p_k,

W_{ij} = a nonnegative weight factor defined as $w_{ij} f_{ij}^2 / \hat{f}_{ij}^2$,

$\hat{f}_{ij}$ = the total ionization score in the ith detector and the jth time bin due to all drivers (for ionization, these are high and low energy n-γ reactions in air and in ground and neutron direct ionization),

w_{ij} = a user-defined nonnegative weight function emphasizing the importance of certain spatial regions (typically, about 10.0 near the ground and decreasing to about 0.25 to 1.0 at 1 km above the ground),

V_{ij} = the variance of score f_{ij}.

Score f_{ij} would be reproduced exactly by integral $f(x_i, y_i, z_i, t_j; p_k)$ if driver functional F were an exact fit to the driver and if the variance associated with Monte Carlo score f_{ij} were zero. In this instance, $P(p_k)$ would be zero. In actuality, functional F is not an exact fit, and variance V is proportional to the square of a fractional deviation averaging about 20 percent for the data given.

It is apparent that minimization of $P(p_k)$ yields a weighted least-squares fit. The use of the inverse of variance V_{ij} increases the weight of low-variance Monte Carlo data, which is expected to be more accurate than high-variance data in inverse proportion to the variance. The use of ratio $f_{ij}^2/\hat{f}_{ij}^2$ causes the relative importance of this driver to be considered in comparison with all the other contributing drivers. If the ratio is small, the weight is diminished accordingly; if the ratio is near unity (that is, no other driver is contributing significantly), the weight is maximized. User-defined factor w_i is used to force the best fit to be obtained near the ground (large w_i) and a moderately good fit far from the ground (small w_i). A very good fit near the ground is desired because most EMP targets (that is, electronic systems) are found on or near the ground.

To evaluate the quadruple integral,

$$f\left(x_i,y_i,z_i,t_j;p_k\right) \equiv \iiint_{V_i} dx\ dy\ dz \int_{t_{j-1}}^{t_j} dt\ F\left(x_i,y_i,z_i,t_j;p_k\right) \quad ,$$

over detector volume V_i and time bin (t_{j-1},t_j), a numerical integration must be done. This numerical integration must be done efficiently because integral f must be evaluated 63 × 19 = 1197 times for each evaluation of penalty function P. Penalty function P must typically be evaluated several hundred times to locate a useful minimum and the associated best fit. Thus, the numerical integration may be required about 10^5 times to complete one of the necessary 4 × 13 × 9 = 468 runs of BIGFIT. This is about 10^7 integral evaluations for the entire fitting problem. Evaluation of functional F requires roughly 10^{-3} s of computer central processor (CP) time, so that about 10^4N seconds of CP time are forecast if N evaluations of functional F are needed to obtain its numerical integral f. Clearly, N must be as near unity as possible to avoid prohibitive computer time requirements. Accordingly, a three-point Gauss-Legendre quadrature was used for the time integration, and a special, highly accurate two-point Gaussian quadrature (with adjustable weight function) was developed by this writer and used for the volume integration. Appendix A describes the two-point scheme. Several other techniques were used to reduce the overall CP time requirement to about 40 hr for the entire curve-fitting project.

With the penalty function thus defined for the driver functional, it is necessary to minimize the penalty function by adjustment of the parameter vector. A highly efficient minimization algorithm is desired, in the sense of using the fewest possible evaluations of the penalty function. A number of different minimization algorithms were tested.

The most efficient algorithm for this application was determined to be a modified conjugate gradient method. This writer adapted the well-known conjugate gradient method[8] to use finite differences to estimate the gradient matrix and to cycle indefinitely during a single descent procedure instead of repeating the descent procedure after cycling once for each element in the vector of independent variables. A very efficient algorithm with quadratic convergence also was developed to search for a minimum along a chosen direction, in connection with the descent procedure. Appendix B contains a listing of the FORTRAN version of these descent algorithms. It was found that minimization of the penalty function proceeded much more rapidly if amplitude parameter p_1 were optimized analytically during evaluation of penalty function $P(p_k)$. Optimum amplitude α (to minimize $P(p_k)$ with respect to the amplitude parameter) can easily be shown to be trial amplitude α_t multiplied by the factor

$$K = \frac{\sum_{i,j} f_{ij} f\left(x_i, y_i, z_i, t_j; p_k\right) g_{ij}}{\sum_{i,j} \left[f\left(x_i, y_i, z_i, t_j; p_k\right)\right]^2 g_{ij}} ,$$

where, as previously explained,

f_{ij} = the data value for volume detector i and time bin j,

$f(\ )$ = the corresponding value of the fit using a nonzero trial value (completely arbitrary) for p_1,

g_{ij} = corresponding complete weight function W_{ij}/V_{ij} used in penalty function $P(p_k)$.

When p_1 is chosen in this way to be $\alpha = K\alpha_t$ and when the minimization of $P(p_k)$ is done for the other p_k exclusive of p_1, the minimization process is greatly accelerated.

Minimizing the penalty function (that is, obtaining the best fit) can be interpreted geometrically as finding the bottom of a hypersurface whose dimensionality is the number of functional parameters. An initial guess for the p_k provides a starting point for the descent. Taking an initial guess that is close to the true bottom reduces the descent effort and helps keep the descent path out of undesirable local minima that are far from the true bottom (that is, the least minimum). Although the computer calculation was performed in double precision, it

[8] *R. Fletcher and C. M. Reeves, Function Minimization by Conjugate Gradients, Computer Journal, 7 (1964), 149-154.*

was learned that a minimum in the hypersurface takes on a rough, granular texture in its shallowest portions due to roundoff errors in the calculation. This undesirable texture impedes the descent to the desired minimum. In general, the speed of descent is slowed by complexity or exceptional shallowness of the hypersurface. Greater complexity is typically caused by more parameters having higher polynomial degree than quadratic (in a Taylor expansion of the penalty function) so that the descent requires more changes in direction. Shallowness increases in rough proportion to the number of scattered data being fitted with the functional. For example, if the number of data is increased tenfold, but the data scatter (due to finite variance) is not reduced, the hypersurface becomes roughly 10 times shallower. It then becomes harder to find the precise bottom of the shallower surface. In this work, the penalty function hypersurface is both complex and shallow, and the success of the fitting process depended critically on the efficiency and the robustness of the minimization procedures.

The initial guesses for the various sets of parameters p_k were usually taken from the optimal values of p_k for adjacent source neutron energy bands or burst heights. After the optimum values for p_k were obtained for a particular descent, the importance of each parameter was tested. If elimination of a parameter caused a sizeable increase in the penalty function, that parameter was deemed important. If a negligible increase was observed, that parameter was deemed unimportant and was removed from the functional. The functionals for several drivers were considerably simplified in this way.

An example of the effect of minimizing the penalty function is shown for one volume detector in table 2. The energy deposition (or ionization) due to thermal neutron capture in the ground is given for volume detector 33, source neutron energy band 9 (8.19 to 15.0 MeV), and 200-m burst height. Detector 33 is 600 to 900 m above the ground at 1200- to 1500-m ground range from the burst. Table 2 gives these parameters:

the time bin boundaries,

f_{ij}, the Monte Carlo score in the detector,

f, the optimal global fit score in the detector,

f_T, the trial global fit score in the detector,

d_{ij}, the percentage of fractional deviation (due to the variance) of the Monte Carlo score for this driver,

$\hat{d}_{ij}$, the percentage of fractional deviation (due to the variance) of the Monte Carlo score for the sum of all drivers,

r, the percentage fraction of the total Monte Carlo score, $\hat{f}_{ij}$, due to this driver, f_{ij} ($r = 100\ f_{ij}/\hat{f}_{ij}$),

e, the percentage of difference between the Monte Carlo score, f_{ij}, and the optimal fit score, f,

$\hat{e}$, the percentage of "error" in the total score contributed by optimal fit score f,

e_T, the percentage of difference between Monte Carlo score f_{ij} and trial fit score f_T,

$\hat{e}_T$, the same as $\hat{e}$, but evaluated for the trial fit score f_T.

The goal of the fitting process is to make e as small as possible in each time bin. When r is larger, a better fit is needed to make e small and thereby make $\hat{e}$ small. Generally, e is desired to be roughly equal to or smaller than d_{ij} for each time bin. Since fractional deviation d_{ij} (due to the variance) is an estimate of the Monte Carlo error, difference e between the fit and the Monte Carlo score should be about equal to d_{ij}. Thus, when d_{ij} is large, e may be large; when d_{ij} is small, e should be small. In table 2, time bins 11 through 13 have d_{ij} averaging 20 to 25 percent and e averaging about 10 percent; time bins 15 through 18 have d_{ij} averaging 40 to 50 percent and e averaging about 40 percent. The values for e and $\hat{e}$ appear to fluctuate approximately randomly about zero in time bins 8 through 19, as would be expected of a good fit to the data. The largest values for e_T and $\hat{e}$ have been reduced by the fitting process to smaller values for e and $\hat{e}$.

TABLE 2. EFFECT OF MINIMIZING PENALTY FUNCTION FOR IONIZATION RATE, VOLUME DETECTOR 33, NEUTRON ENERGY BAND 9 (8.19 TO 15.0 MeV), 200-m BURST HEIGHT

Time bin	Start of time bin (s)	f_{ij}	f	f_T	d_{ij}	$\hat{d}_{ij}$	r	e	$\hat{e}$	e_T	$\hat{e}_T$
1	0.0	0.0	0.8902D-12	0.9283D-12	99.9	9.3	0.0	100.0	0.0	100.0	0.0
2	0.1000D-06	0.7037D-08	0.3749D-11	0.3910D-11	99.9	10.8	0.1	-99.9	-0.1	-99.9	-0.1
3	0.2150D-06	0.0	0.8655D-11	0.9026D-11	99.9	11.4	0.0	100.0	0.0	100.0	0.0
4	0.4640D-06	0.0	01905D-10	0.1987D-10	99.9	10.9	0.0	100.0	0.0	100.0	0.0
5	0.1000D-05	0.0	0.4053D-10	0.4228D-10	99.9	9.9	0.0	100.0	0.0	100.0	0.0
6	0.2150D-05	0.0	0.8309D-10	0.8671D-10	99.9	10.6	0.0	100.0	0.0	100.0	0.0
7	0.4640D-05	0.0	0.1588D-09	0.1659D-09	99.9	9.4	0.0	100.0	0.0	100.0	0.0
8	0.1000D-04	0.3858D-09	0.2659D-09	0.2780D-09	78.2	11.7	0.2	-31.1	-0.1	-27.9	-0.1
9	0.2150D-04	0.3121D-09	0.3653D-09	0.3814D-09	76.7	7.1	0.3	14.6	0.0	18.2	0.1
10	0.4640D-04	0.2202D-09	0.4027D-09	0.4155D-09	64.9	9.0	1.0	45.3	0.4	47.0	0.5
11	0.1000D-03	0.3823D-09	0.3606D-09	0.3580D-09	17.6	9.6	7.0	-5.7	-0.4	-6.4	-0.4
12	0.2150D-03	0.2123D-09	0.2503D-09	0.2255D-09	20.9	9.2	26.8	15.2	4.1	5.9	1.6
13	0.4640D-03	0.1282D-09	0.1143D-09	0.8529D-10	29.3	23.7	80.6	-10.8	-8.7	-33.5	-27.0
14	0.1000D-02	0.3546D-10	0.3013D-10	0.1921D-10	69.2	58.4	83.7	-15.0	-12.6	-45.8	-38.3
15	0.2150D-02	0.6082D-11	0.8749D-11	0.6371D-11	43.6	36.6	63.4	30.5	19.3	4.5	2.9
16	0.4640D-02	0.2689D-11	0.3813D-11	0.2867D-11	50.3	28.7	13.9	29.5	4.1	6.2	0.9
17	0.1000D-01	0.3794D-11	0.1688D-11	0.1283D-11	39.2	25.5	27.7	-55.5	-15.4	-66.2	-18.3
18	0.2150D-01	0.1349D-11	0.7428D-12	0.5717D-12	52.4	15.5	15.8	-44.9	-7.1	-57.6	-9.1
19	0.4640D-01	0.3319D-12	0.3262D-12	0.2542D-12	35.0	17.5	7.6	-1.7	-0.1	-23.4	-1.8

Notes:

f_{ij} = *the Monte Carlo score in the detector.*

f = *the optimal global fit score in the detector.*

f_T = *the trial global fit score in the detector.*

d_{ij} = *the percentage of fractional deviation (due to the variance) of the Monte Carlo score for these drivers.*

$\hat{d}_{ij}$ = *the percentage of fractional deviation (due to the variance) of the Monte Carlo score for the sum of all drivers.*

r = $100\ f_{ij}/\hat{f}_{ij}$.

e = *the percentage of difference between* f_{ij} *and* f.

$\hat{e}$ = $re/100$.

e_T = *the percentage of difference between* f_{ij} *and* f_T.

$\hat{e}_T$ = $re_T/100$.

6. BURST HEIGHT DEPENDENCE OF FIT PARAMETERS

Having obtained parameter values at four burst heights, we desired to develop smooth functions of burst height to approximate the parameter values. Some scatter was evident in the burst height dependence. The functions chosen should avoid reproducing the scatter, but capture the important trend of the data. Two burst height functions were selected: (1) the constant function, independent of burst height, and (2) the rational function

$$g(h) = \frac{C_1 + C_2 h + C_3 h^2}{1 + C_4 h^2} \quad ,$$

where h is the burst height and C_i are fit coefficients. By inspection of the parameter values at the four burst heights, the author determined which of the two burst height functions was appropriate for a parameter. Many parameters were clearly independent of burst height. Other parameters displayed such severe scatter that it was necessary to use merely an average value for all burst heights. On the other hand, many parameters showed well-defined trends and were fitted with rational functions.

Fitting the four values of a parameter with a rational function was not a trivial problem. In its application to real EMP prediction problems, the rational function would be evaluated at other burst heights. Therefore, the behavior of the rational function must be carefully controlled for all possible burst heights. For example, simply fitting the four parameter values with rational function g(h) would reproduce the data exactly, but might introduce poles, crossovers, and similar erratic behavior at other burst heights. To avoid this possibility, several strategems were adopted. First, the fit was to be done by use of Courant's well-known penalty function method for optimization with nonlinear constraints, and the nonlinear constraints would be defined so as to inhibit the erratic behavior. Second, the rational function would be made to fit not the four data, but the piecewise linear function $\hat{p}$ interpolating the four data.

The penalty function used was

$$Q(C_i; r) = \sum_j \left[g(h_j) - \hat{p}(h_j) \right] + r(N_1 + N_2 + N_3) \quad .$$

The h_j are about 40 burst heights on the interval from 1 to 300 m. N_1, N_2, and N_3 are positive semidefinite functions that are zero when a corresponding constraint is satisfied. In the optimization process, Q is minimized for successively larger values of r by using as each starting point the previous optimum values for C_i. As r is increased to infinity, Q becomes optimal for the constraints represented by N_1, N_2, and N_3. The specific nonlinear constraints were these:

a. For complex h, no poles of g(h) in the right half-plane of h,

$$N_1 = 10^8[\min(0,C_4)]^2 \quad ,$$

b. No crossover to negative values of g(h) for large h,

$$N2 = 10^8[\min(0,C3)]^2/\hat{p}(200\ m) \quad ,$$

c. No negative values for g(h) for small h,

$$N_3 = [\min(0,C_1)]^2/\hat{p}(200\ m) \quad .$$

The minimization of Q was done for each value of r by adjusting the four C_i. The descent algorithms described in section 5 were used. For burst heights above 200 m, most driver parameters tend toward limiting values not much different from the value at the 200-m burst height. An exception is the amplitude parameter for a ground-induced source. This parameter should decay monotonically to zero as the burst height increases. For burst heights above 250 m, the three high-energy ground driver amplitudes are made to decay by a factor of two for each additional 100 m. Similarly, the three low-energy ground driver amplitudes are made to decay by a factor of 1.2 to 4, depending on the source neutron energy, fcr each additional 100-m increase in burst height over 250 m.

7. COMPARISON WITH LIQUID AIR EXPERIMENT

Sidhu et al[9] measured neutron and secondary gamma ray transport through a liquid air sphere for a 14-MeV neutron source. Their 129.3-cm sphere radius was equivalent to an atmospheric range of 850 m. They published (their fig. 7) for secondary gamma rays a value of about 1.3×10^{-10} cm^2-rad (tissue)/source neutron for the $4\pi r^2$ dose at 850-m equivalent range in air. The corresponding value for the NEMP code energy band 9 (8.19 to 15.0 MeV) high-energy air driver is 1.5×10^{-10} cm^2-rad (air). One rad in tissue and one rad in air differ by only about 1 percent, so these gamma doses differ by about 15 percent.

[9] *G. S. Sidhu, W. E. Farley, L. F. Hansen, T. Komoto, B. Pohl, and C. Wong, Transport of Neutron and Secondary Gamma Radiations Through a Liquid Air Sphere Surrounding a 14-MeV Neutron Source, Nuclear Science and Engineering, 66 (June 1978), 428-433.*

The NEMP neutron dose in air cannot be compared easily with the measured neutron tissue dose because neutron kerma* factors are very energy dependent in the range from 1 to 14 MeV. The neutron energy spectrum at the 850-m observer for the NEMP driver is unavailable to allow a conversion fron neutron air dose to neutron tissue dose.

Shown in figure 7 of Sidhu et al[9] are results of TARTNP computer code calculations of the gamma tissue dose. The TARTNP code is a discrete ordinates radiation transport code used at the Lawrence Livermore Laboratories. The results show the $4\pi r^2$ dose to a 2800-m range. Differences between the NEMP driver and TARTNP results appear to be small (a few percent) from 850 to 2500 m. The NEMP code results are roughly 15 pecent lower at the 500-m range.

8. COMPARISON WITH EARLIER APPROXIMATION FOR IONIZATION BY 14-MeV NEUTRONS

Longley et al[5] developed approximations for EMP drivers for use in their LEMP 2 surface burst EMP environment prediction code. They used Longmire's analytic first-scatter theory and many-scatter diffusion theory to describe 14-MeV neutron direct ionization through elastic scattering and (n,p) reactions. Comparison of their 14-MeV neutron driver with the corresponding NEMP driver (energy band 9, direct neutron ionization) showed rough agreement and some differences. For dose in air, the NEMP results exhibited a 10-percent longer attenuation length at all ranges and a roughly 50-percent greater amplitude (factoring out the range dependence). Because detailed reaction cross sections were not used for this LEMP 2 driver (per C. L. Longmire, Mission Research Corp.), some disagreement is expected.

Since the LEMP 2 drivers are independent of the source neutron energy spectrum (except for 14-MeV neutrons), a comparison with the nine energy band NEMP drivers is a complicated undertaking beyond the scope of this report.

---

[5] *H. J. Longley, C. L. Longmire, J. S. Malik, R. M. Hamilton, R. N. Marks, and K. S. Smith, Development and Testing of LEMP 2, A Surface Burst EMP Code (U), Mission Research Corp., Santa Barbara, CA, DNA 4097T (December 1976). (CONFIDENTIAL)*

[9] *G. S. Sidhu, W. E. Farley, L. F. Hansen, T. Komoto, B. Pohl, and C. Wong, Transport of Neutron and Secondary Gamma Radiations Through a Liquid Air Sphere Surrounding a 14-MeV Neutron Source, Nuclear Science and Engineering, 66 (June 1978), 428-433.*

**The total kinetic energy of directly ionizing particles ejected by the action of indirectly ionizing radiation per unit mass of specified material.*

9. SELECTED RESULTS

Time histories of some NEMP neutron-induced EMP drivers are portrayed in figures 2 to 13. Radial Compton current, theta Compton current, and ionization rate are plotted. Results are shown for two observers 0 and 500 m above the ground for each of two burst heights of 1 and 200 m. The ground range from the burst to the observer is 1000 m. All results are for a source of one neutron in the energy band of 8.19 to 15.0 MeV. Although drivers for other neutron energy bands have different amplitudes, attenuation lengths, burst height dependence, air-ground interface effects, etc., these results are typical.

In the figures, each driver is represented by a broken line with identifying symbols. The "F" denotes the high-energy ground driver (ground inelastics); the "I" denotes the high-energy air driver (air inelastics); the "G" denotes the low-energy ground driver (ground captures); the "A" denotes the low-energy air driver (air captures); and the "N" denotes neutron direct ionization including charged particle ionization. The total for all drivers is represented by a solid line with identifying "T" symbols. Each curve is the magnitude, or absolute value, of the driver or total.

Several general observations can be made concerning burst height and observer height variations. High-energy ground drivers are significantly weaker for greater burst heights. Low-energy ground drivers decay more slowly with increasing burst height than do high-energy ground drivers because source neutrons penetrate to greater ranges while decaying to lower energies. Low- and high-energy air drivers and the neutron direct ionization driver all are roughly twice as strong for the 200-m burst height as for the 1-m burst height because roughly half of the source neutrons are absorbed by the ground for the lower burst height.

The drivers for theta Compton current are all stronger for observers closer to the ground surface because of the asymmetry presented by the air-ground interface. High-energy and low-energy air drivers for radial Compton current and ionization rate are relatively insensitive to observer height. The time dependence of the neutron direct ionization driver is different for the two observer heights considered. This driver is somewhat shorter in duration near the ground because many later-arriving multiply scattered neutrons tend to become trapped in the ground and do not contribute to the driver in the air. The low-energy

ground driver for ionization rate is somewhat stronger for the higher observer, more noticeably so for the 200-m burst height than for the 1-m burst height. They differ because the secondary gamma rays (produced by neutron capture in the ground) that drive the ionization rate at the observer must penetrate more soil to reach the shallower observer. The low-energy ground driver for radial Compton current is even more strongly decreased for observers near the ground because the net Compton current flow follows the direction of the gamma ray flux, which is predominantly up out of or down into the ground (perpendicular to the radial direction). Higher off the ground, more gamma rays with a nearly radial direction arrive from ground regions close to the burst.

All drivers contributing to the radial Compton current have the same sign (negative). The theta Compton current drivers may have different signs or even change sign. (By convention, positive is downward.) The theta Compton currents for high-energy ground and low-energy air drivers are positive and negative, respectively. The theta Compton current for the low-energy ground driver is generally negative at this range from the burst because of a secondary gamma ray "fountain" effect. This effect is due to many secondary gamma rays rising upward from the ground close to the burst and being turned down toward the ground after a few Compton collisions in the air. However, for observers close to the ground and close to the burst, enough upward-going secondary gamma rays are produced beneath the observer to reverse the theta Compton current from negative to positive for a period of time (fig. 9). The theta Compton current for high-energy air reactions was set identically to zero because it was about two orders of magnitude smaller than the corresponding radial Compton current and because the available Monte Carlo statistics for those data were so poor that a reliable fit was unlikely.

The time history of the high-energy ground drivers for theta Compton current and ionization rate deserves some explanation. It may consist of two pulses: one from the initial arrival of neutrons at the ground beneath the burst and the other from the arrival of neutrons at an area roughly midway between the burst and the observer. The secondary gamma rays produced in the ground have an attenuation length considerably greater than the mean free path of the neutrons. This greater length causes contributions from reactions (per unit ground surface area) beneath the burst to be more important than contributions from reactions very near the observer. However, gamma rays originating in the ground closer to the observer are less attenuated by the ground because of their higher angle of departure from the ground. This complicated

behavior was approximated by the two pulses mentioned. The approximation gives reasonable agreement with the Monte Carlo data, but too much importance should not be attached to the detailed structure of the time history approximation, expecially since the data time bins were one-third of an order of magnitude wide. The second pulse of this two-pulse structure is not observed in the data (and the driver) for radial Compton current. Also, the second pulse is not observed in the data (and the driver) for ionization rate if the burst height is very near the surface (fig. 4 and 7) or if the observer is very high (fig. 13).

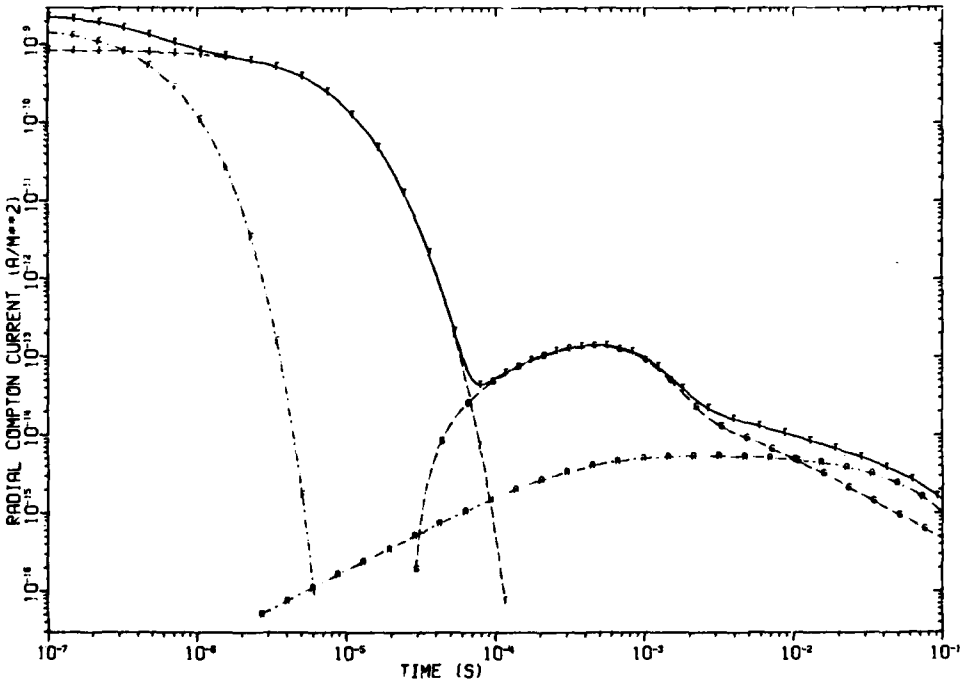

Figure 2. Radial Compton current for 1-m burst height, 0-m observer height, and 1000-m ground range.

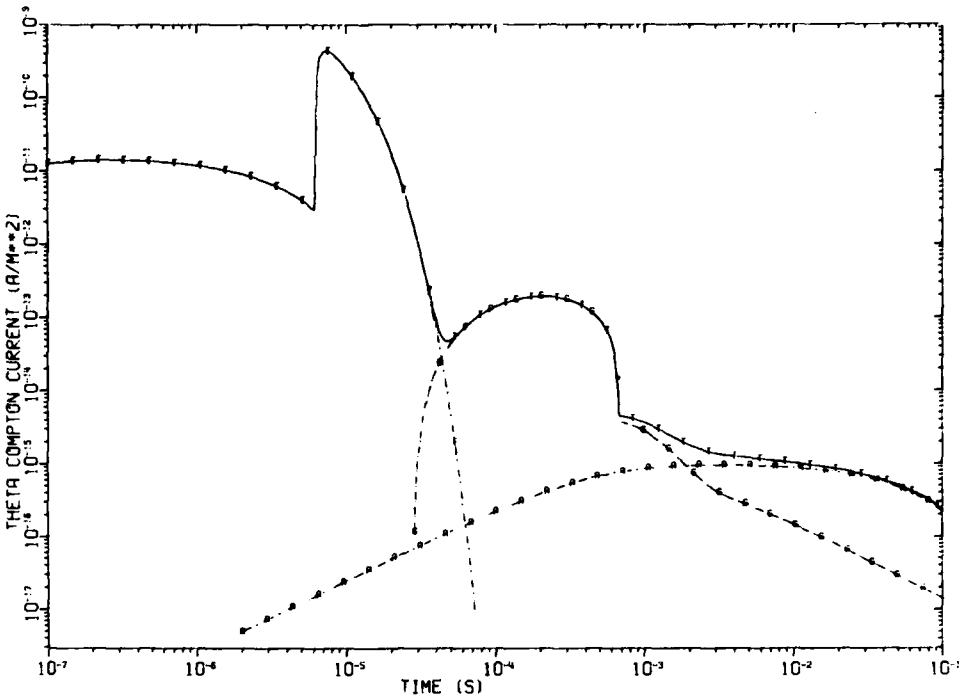

Figure 3. Theta Compton current for 1-m burst height, 0-m observer height, and 1000-m ground range.

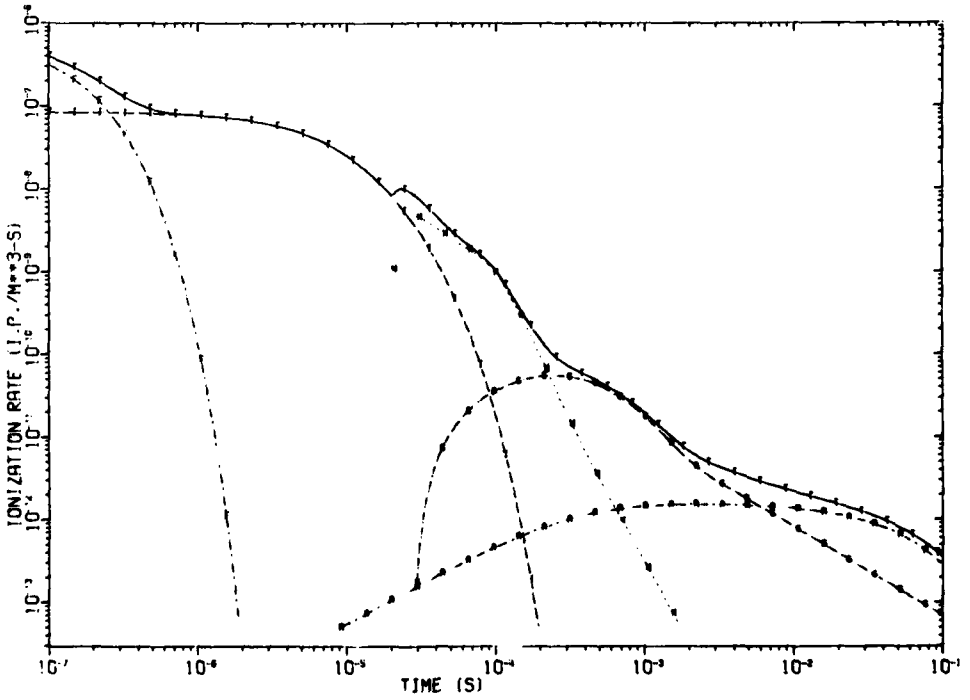

Figure 4. Ionization rate for 1-m burst height, 0-m observer height, and 1000-m ground range.

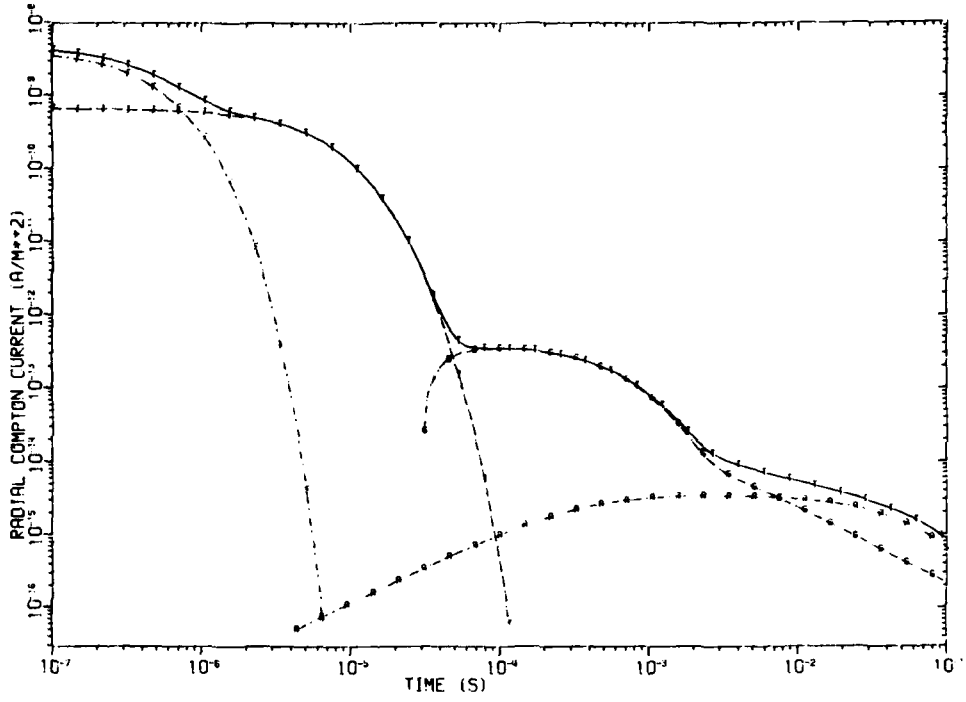

Figure 5. Radial Compton current for 1-m burst height, 500-m observer height, and 1000-m ground range.

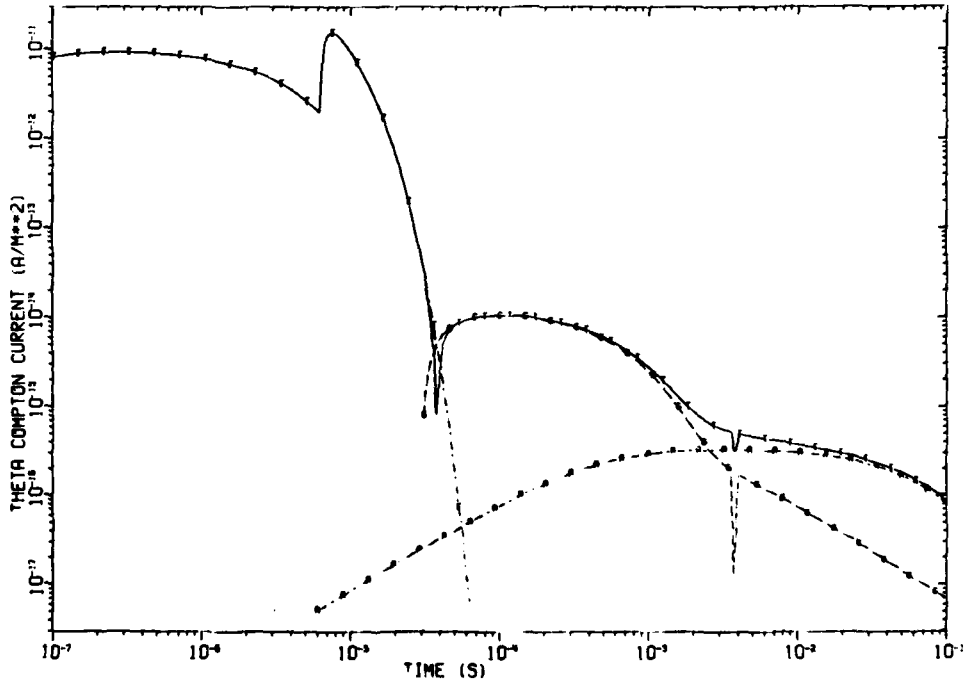

Figure 6. Theta Compton current for 1-m burst height, 500-m observer height, and 1000-m ground range.

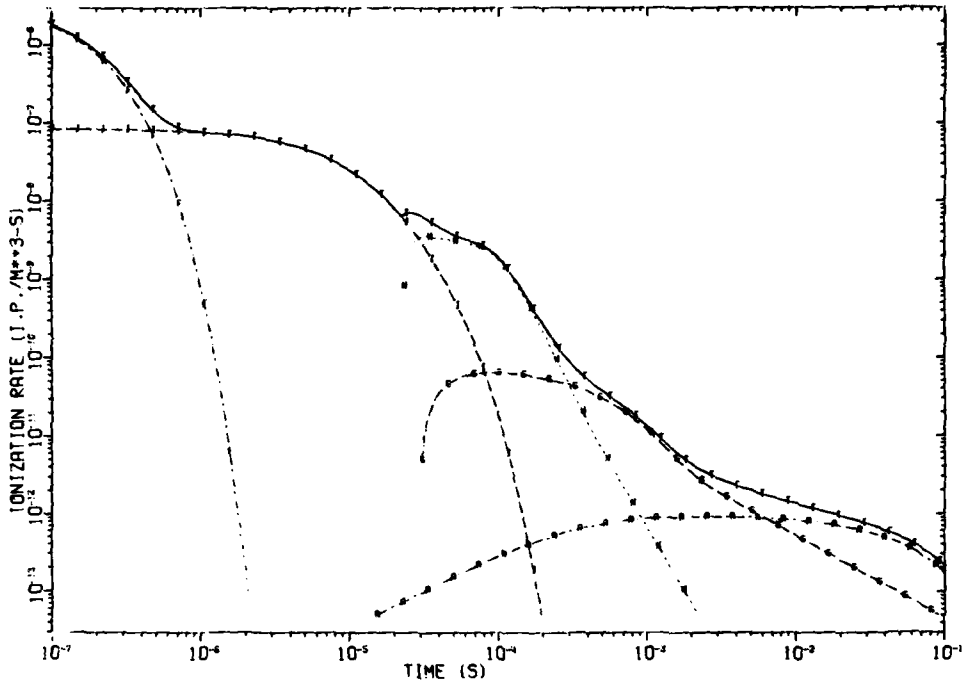

Figure 7. Ionization rate for 1-m burst height, 500-m observer height, and 1000-m ground range.

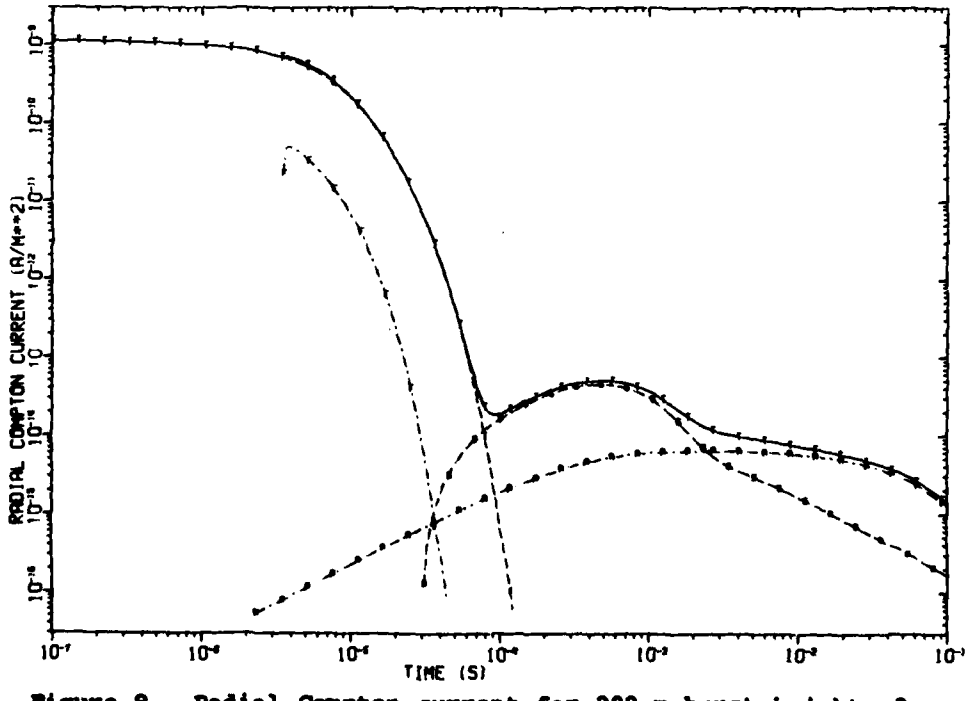

Figure 8. Radial Compton current for 200-m burst height, 0-m observer height, and 1000-m ground range.

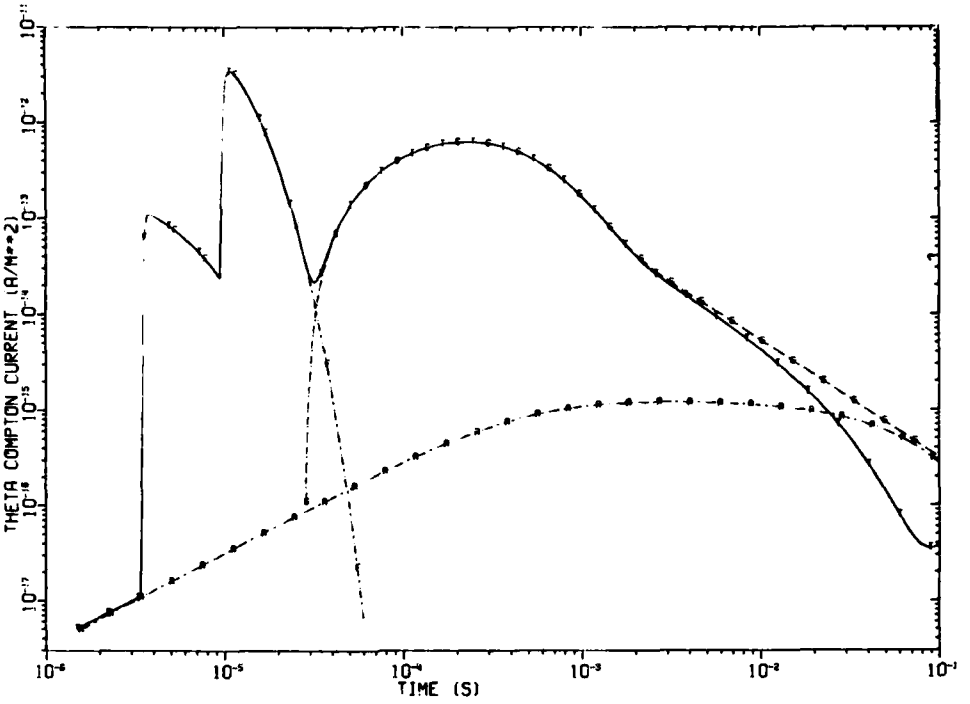

Figure 9. Theta Compton current for 200-m burst height, 0-m observer height, and 1000-m ground range.

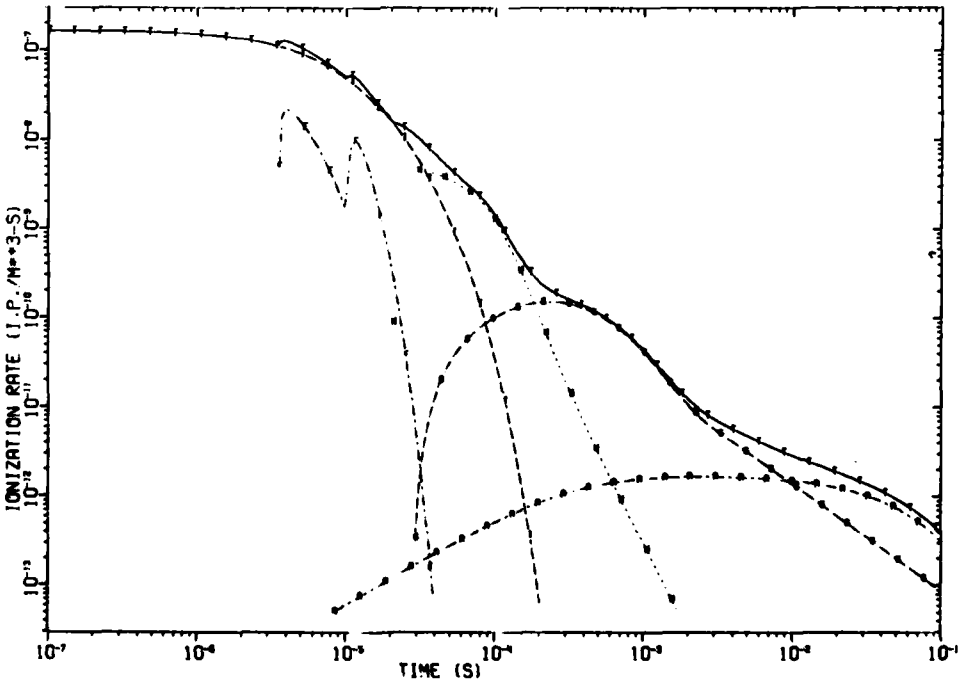

Figure 10. Ionization rate for 200-m burst height, 0-m observer height, and 1000-m ground range.

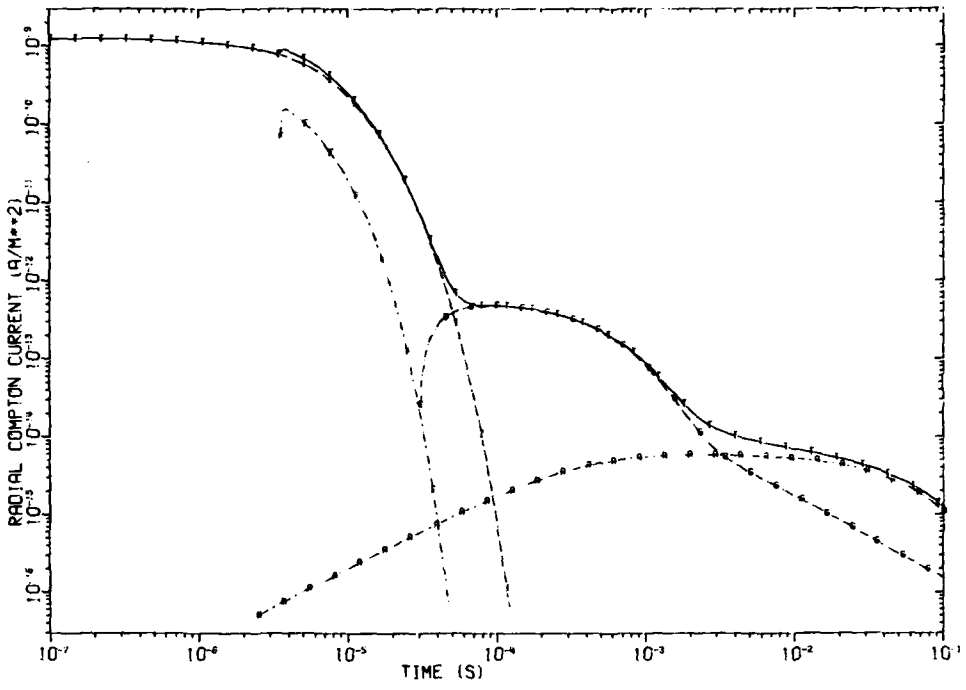

Figure 11. Radial Compton current for 200-m burst height, 500-m observer height, and 1000-m ground range.

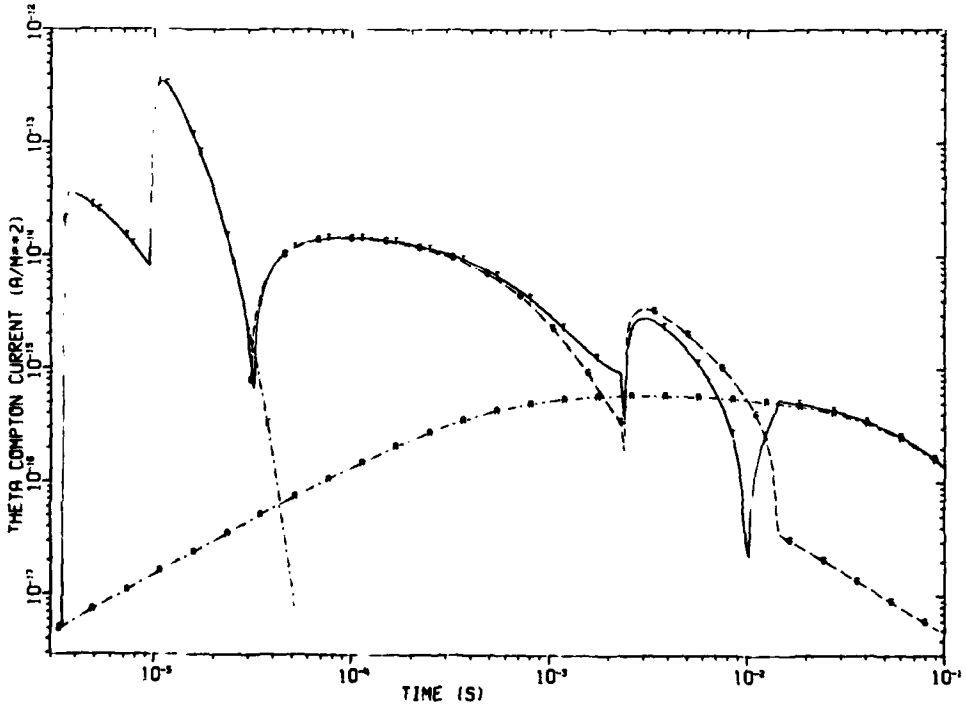

Figure 12. Theta Compton current for 200-m burst height, 500-m observer height, and 1000-m ground range.

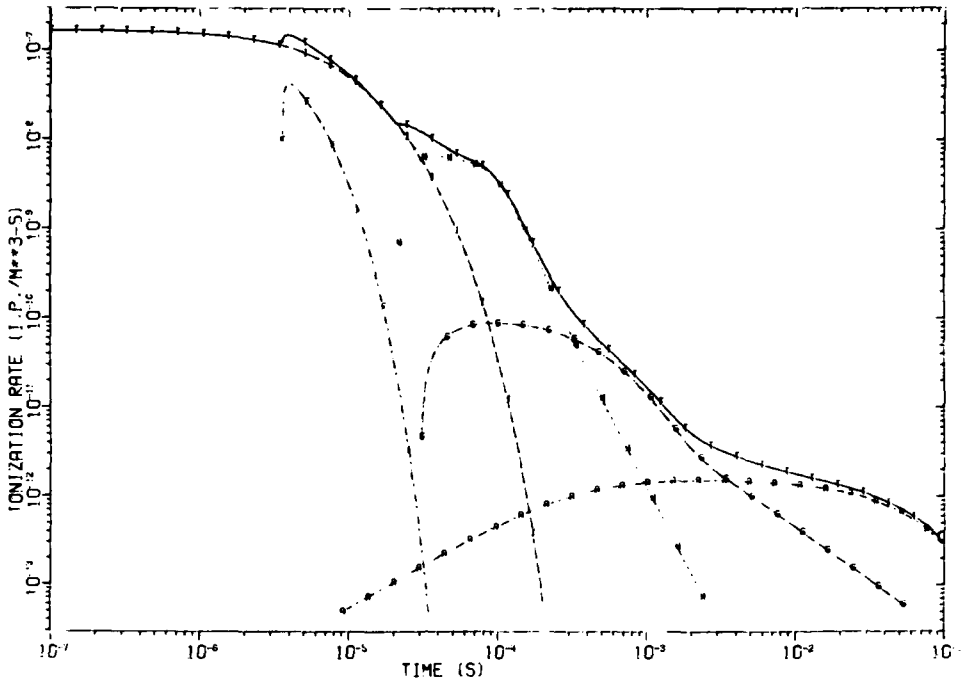

Figure 13. Ionization rate for 200-m burst height, 500-m observer height, and 1000-m ground range.

10. CONCLUSIONS

The NEMP neutron-induced EMP driver package represents the state of the art for predicting EMP drivers from near-surface bursts, allowing flexible representation of any weapon's neutron energy spectrum and choice of any burst height in the near-surface regime. The package consists of separate space- and time-dependent drivers for radial and theta Compton current and ionization rate, for high- and low-energy reactions in the air and the ground, for nine source neutron energy bands, for any near-surface burst height.

This report has described the development of this EMP driver package for neutron-induced sources, for use in the NEMP code for EMP environment prediction for near-surface nuclear bursts. The development was based on the concept of obtaining a global fit of certain well-chosen functionals to Monte Carlo transport data over the entire set of volume detectors and time bins. The global fit obtained in this manner offered several advantages over fitting with polynomials, including the effective elimination of Monte Carlo "noise" and the possibility of reduction of error below the level of Monte Carlo statistical error. The fit also involved far fewer degrees of freedom. The global fit was obtained by minimization of a penalty function representing the badness

of fit. Because of the large amount of computer time involved, highly efficient minimization algorithms were employed. The difficulty of the minimization depended, among other things, on the variance of the Monte Carlo data, which averaged about 20 to 30 percent. The burst height dependence of the fit parameters was explicitly obtained for burst heights from 1 to 250 m. Extrapolation methods were devised for burst heights greater than 250 m.

Comparison of ionization from gamma rays induced by a 14-MeV neutron source with experimental measurements gave good agreement. Comparison with the LEMP 2 direct neutron ionization driver for 14-MeV neutrons revealed significant differences. Typical results were discussed for two burst heights and two observer heights, for the 8.19- to 15.0-MeV source neutron energy band drivers.

LITERATURE CITED

(1) William T. Wyatt, Jr., A Near-Surface Burst EMP Driver Package for Prompt Gamma-Induced Sources, Harry Diamond Laboratories HDL-TR-1931 (September 1980).

(2) H. J. Longley, C. L. Longmire, and K. S. Smith, Development of NEMP (U), Mission Research Corp., Santa Barbara, CA, HDL-CR-75-001-1 (April 1975). (SECRET--RESTRICTED DATA)

(3) H. J. Longley and K. S. Smith, Developments in NEMP for 1977 (U), Mission Research Corp., Santa Barbara, CA, HDL-CR-77-0022-1 (January 1978). (SECRET--RESTRICTED DATA)

(4) H. J. Longley and C. L. Longmire, Development and Testing of LEMP 1, Los Alamos Scientific Laboratory, NM, LA-4346 (April 1970).

(5) H. J. Longley, C. L. Longmire, J. S. Malik, R. M. Hamilton, R. N. Marks, and K. S. Smith, Development and Testing of LEMP 2, A Surface Burst EMP Code (U), Mission Research Corp., Santa Barbara, CA, DNA 4097T (December 1976). (CONFIDENTIAL)

(6) D. A. Sargis, E. R. Parkinson, J. N. Wood, R. E. Dietz, and C. A. Stevens, Late-Time Sources for Close-In EMP, Science Applications, Inc., La Jolla, CA, DNA 3064F (August 1972).

(7) H. S. Schechter and M. O. Cohen, Energy Deposition Rates and Compton Electron Currents from Low-Altitude Bursts as a Function of Source Energy, Mathematical Applications Group, Inc., Elmsford, NY, HDL-CR-77-020-1 (November 1977)

(8) R. Fletcher and C. M. Reeves, Function Minimization by Conjugate Gradients, Computer Journal, 7 (1964), 149-154.

(9) G. S. Sidhu, W. E. Farley, L. F. Hansen, T. Komoto, B. Pohl, and C. Wong, Transport of Neutron and Secondary Gamma Radiations Through a Liquid Air Sphere Surrounding a 14-MeV Neutron Source, Nuclear Science and Engineering, 66 (June 1978), 428-433.

APPENDIX A.--A TWO-POINT QUADRATURE SCHEME

Integrating a driver functional over the entire volume of a volume detector can be very time-consuming if unsophisticated quadrature methods are used. The volume detector concerned is a square toroid, that is, a toroid with a square cross section in coordinates (x,z,ϕ). The toroid is bounded by X_1, X_2, Z_1, and Z_2, where x is the ground range from the coordinate center and z is the height above the ground. The driver has azimuthal symmetry around the center of the toroid (x = 0) so that an integration in independent variable ϕ is trivial. Thus, an integral over detector volume

$$I = \int_{X_1}^{X_2} \int_{Z_1}^{Z_2} \int_0^{2\pi} f(x,z)\left(x^2 + z^2\right)^{1/2} dx\ dz\ d\phi$$

becomes

$$I = 2\pi \int_{X_1}^{X_2} \int_{Z_1}^{Z_2} f(x,z)\left(x^2 + z^2\right)^{1/2}\ dx\ dz \quad .$$

If f(x,z) describes a driver functional, the salient spatial gradients of f(x,z) are (1) in the vertical (z > 0) direction due to proximity of the ground and (2) in the radial direction from the burst due to geometric and atmospheric attenuation. A particularly accurate Gaussian quadrature rule would use the geometric and atmospheric attenuation as a weight function.

Our goal is a Gaussian quadrature rule for the integral

$$J = \int_{X_1}^{X_2} \int_{Z_1}^{Z_2} v(x,z)w(x,z;\alpha)\ dx\ dz \quad ,$$

where v is a function of x and y and w is a weight function defined by

$$w(x,z;\alpha) = \exp(-\alpha r)/\left(1 + r^2\right) \quad ,$$

$$r = \left[x^2 + (z - h)^2\right]^{1/2} \quad .$$

The burst height is h. The advantage of this weight function rests on the fact that it represents the actual spatial dependence (for a suitable choice of α) better than a low-order power series would. Parameter α is essentially the atmospheric attenuation coefficient (the reciprocal of the attenuation length) and is available for use during

the calculation of a driver integral. Thus, we may exploit our knowledge of α to construct the quadrature based on weight function $w(x,z;\alpha)$. In computer program BIGFIT, we actually first construct a family of quadrature rules for a range of values α_i. Then when a driver integral is being calculated, the α_i nearest to α is determined, and its corresponding quadrature rule is used. In this way, the construction of the quadrature rules is kept out of the inner program loops.

For the J integral quadrature rule, we seek quadrature points (x_1,z_1) and (x_1,z_2) with weight coefficients w_1 and w_2, respectively. We require exact integration of Taylor series terms for x^0 (and z^0), x^1,z^1,z^2, and z^3. This requirement yields the following conditions on x_1,z_1,z_2,w_1, and w_2:

$$w_1 + w_2 = M_{00} \quad ,$$

$$w_1x_1 + w_2x_1 = M_{10} \quad ,$$

$$w_1z_1 + w_2z_2 = M_{01} \quad ,$$

$$w_1z_1^2 + w_2z_2^2 = M_{02} \quad ,$$

$$w_1z_1^3 + w_2z_2^3 = M_{03} \quad ,$$

where

$$M_{ij} = \int_{x_1}^{x_2} \int_{z_1}^{z_2} x^i z^j w(x,z;\alpha)\, dx\, dz \quad .$$

This quadrature is separable in x and z and easy to obtain. Obviously,

$$x_1 = M_{10}/M_{00} .$$

Define the polynomial

$$P = (z - z_1)(z - z_2) = 0 \quad ,$$

or

$$P = z^2 - Az + B = 0 \quad .$$

Multiply the preceding equations by A and B and add:

$$w_1 B + w_2 B = BM_{00}$$

$$w_1(Az_1) + w_2(Az_2) = AM_{01}$$

$$w_1\left(z_1^2\right) + w_2\left(z_2^2\right) = M_{02}$$

$$w_1(P) + w_2(P) = AM_{01} + BM_{00} + M_{02}$$

$$w_1 z_1(B) + w_2 z_2(B) = BM_{01}$$

$$w_1 z_1(Az_1) + w_2 z_2(Az_2) = AM_{02}$$

$$w_1 z_1\left(z_1^2\right) + w_2 z_2\left(z_2^2\right) = M_{03}$$

$$w_1 z_1(P) + w_2 z_2(P) = AM_{02} + BM_{01} + M_{03} \quad .$$

Since P = 0, we have

$$AM_{01} + BM_{00} + M_{02} = 0 \quad ,$$

$$AM_{02} + BM_{01} + M_{03} = 0 \quad ,$$

or solving for A and B,

$$A = \left(M_{03}M_{00} - M_{02}M_{01}\right)/C \quad ,$$

$$B = \left(M_{02}^2 - M_{01}M_{03}\right)/C \quad ,$$

where

$$C = M_{01}^2 - M_{00}M_{02} \quad .$$

Therefore,

$$z_1 = \left[-A - \left(A^2 - 4B\right)^{1/2}\right]/2 \quad ,$$

$$z_2 = \left[-A + \left(A^2 - 4B\right)^{1/2}\right]/2 \quad .$$

Then

$$w_1 + w_2 = M_{00} \quad ,$$

$$w_1 z_1 + w_2 z_2 = M_{01} \quad ,$$

or

$$w_1 = (M_{01} - M_{00} z_2)/(z_1 - z_2) \quad ,$$

$$w_2 = M_{00} - w_1 \quad .$$

Suppose we seek to integrate

$$K = \int_{x_1}^{x_2} \int_{z_1}^{z_2} \mu(x,z)\, dx\, dz \quad ,$$

where $\mu(x,z)$ has dominant spatial variation $w(x,z;\alpha)$. We rewrite K as

$$K = \iint \left[\frac{\mu(x,z)}{w(x,z;\alpha)}\right] w(x,z;\alpha)\, dx\, dz$$

and apply the quadrature rule developed to get

$$k \approx w_1 \left[\frac{\mu(x_1,z_1)}{w(x_1,z_1;\alpha)}\right] + w_2 \left[\frac{\mu(x_1,z_2)}{w(x_1,z_2;\alpha)}\right] .$$

It is best to combine $w(x_1,z_1;\alpha)$ with w_1 and $w(x_1,z_2;\alpha)$ with w_2 to obtain the modified rule

$$K \approx \hat{w}_1 \mu(x_1,z_1) + \hat{w}_2 \mu(x_1,z_2) \quad ,$$

where

$$\hat{w}_1 = w_1/w(x_1,z_1;\alpha) \quad ,$$

$$\hat{w}_2 = w_2/w(x_1,z_2;\alpha) \quad .$$

Thus, a unique quadrature rule ($x_1, z_1, z_2, \hat{w}_1$, and $\hat{w}_2$) was obtained for each combination of volume detector and α_i before commencing the descent algorithm to fit a driver functional to Monte Carlo data. Then during the descent, the numerical integration of K-like integrals proceeded extremely rapidly.

APPENDIX B.--DESCENT ALGORITHMS USED

This appendix lists the FORTRAN version of the descent algorithms used to search for a minimum of a function.

APPENDIX B

```
      SUBROUTINE TALCG(FN,X,TOL,B,G,XOLD,STEP,VAL,M,NFN)
C
C                          -- BY WILLIAM T. WYATT, JR., 1978.
C
C  USING THE METHOD OF CONJUGATE GRADIENTS, THIS SUBROUTINE SEARCHES FOR
C  THE MINIMUM OF THE SCALAR FUNCTION  FN , GIVEN A STARTING POINT  X .
C  X  IS A VECTOR OF LENGTH  M .  AN ELEMENT OF  X  IS NOT ALTERED
C  DURING THE SEARCH IF THE CORRESPONDING ELEMENT OF  TOL  IS NON-
C  POSITIVE.  OTHERWISE, THE SEARCH CONTINUES UNTIL THE FUNCTION DOES
C  NOT DECREASE WHEN  X  IS CHANGED BY AS MUCH AS  TOL*STEP , WHERE THE
C  LARGEST ELEMENT IN  STEP  IS UNITY.
C
C  THE SEARCH MAY BE ABORTED AFTER ABOUT  NFN  EVALUATIONS OF THE
C  FUNCTION  FN  IF  NFN>0 , OR AFTER  -NFN  GRADIENT EVALUATIONS IF
C  NFN<0 .
C
C  THE FUNCTION  FN  MUST BE DECLARED  EXTERNAL  IN THE CALLING PROGRAM.
C  X ,  TOL ,  M , AND  NFN  MUST BE DEFINED WHEN THIS SUBROUTINE IS
C  CALLED.  THE SUBROUTINE RETURNS THE MINIMUM LOCATION IN  X , THE
C  MINIMUM FUNCTION VALUE IN  VAL , AND THE NUMBER OF FUNCTION
C  EVALUATIONS IN  ABS(NFN) .  NFN  IS RETURNED NEGATIVE IF THE SEARCH
C  IS ABORTED AS DESCRIBED ABOVE.  THE ARRAYS  B ,  G ,  XOLD , AND
C  STEP  OF LENGTH  M  ARE USED FOR INTERMEDIATE RESULTS.  TOL  AND  M
C  ARE RETURNED UNCHANGED.
C
C  THE PROGRAM CALLS THE SUBROUTINE QUAD TO LOCATE A MINIMUM ALONG A
C  GIVEN DIRECTION.
C
C  AN ELEMENT OF  X  MAY BE COMPELLED TO REMAIN POSITIVE DURING THE
C  SEARCH, BY USING THE TWO STATEMENTS (MARKED WITH "CCCCC") IN THE
C  PROGRAM BELOW:
C                              TOL(I)=-TOL(I)
C                              GO TO 5
C
C  THE METHOD ESTIMATES THE FUNCTION GRADIENT BY FINITE DIFFERENCES OVER
C  AN INTERVAL  TOL*SLASH .  SLASH  HAS BEEN SET TO 0.01 IN A  DATA
C  STATEMENT.  ROUNDOFF ERRORS WILL CAUSE POOR ESTIMATES FOR THE
C  GRADIENT IF  TOL  IS TOO SMALL OR IF MACHINE PRECISION IS
C  INSUFFICIENT.  (DOUBLE PRECISION IS RECOMMENDED FOR COMPUTERS WITH
C  DEFAULT SHORT PRECISION WORDS.)
C
C
      DIMENSION X(M),TOL(M),B(M),G(M),XOLD(M),STEP(M)
      DATA SLASH /0.01/
C
C  INITIALIZE GRADIENT AND DIRECTION ARRAYS AND OTHER QUANTITIES.
      MAXFN=NFN
      NFN=0
      IPASS=0
5     CONTINUE
      DO 10 I=1,M
      B(I)=0.0
10    G(I)=1.0
      VAL=FN(X)
      NFN=NFN+1
C
C
C  MINIMIZATION LOOP BEGINS HERE.  CHECK FOR MAX FN EVALUATIONS.
100   CONTINUE
```

```
      IPASS=IPASS+1
      IF(IPASS.GT.-MAXFN.AND.MAXFN.LT.0) GO TO 900
      IF(NFN.GT.MAXFN.AND.MAXFN.GT.0) GO TO 900
C
C  FIRST, MOVE X TO XOLD.
      SUMOLD=0.0
      DO 110 I=1,M
      XOLD(I)=X(I)
110   SUMOLD=SUMOLD+G(I)**2
      IF(SUMOLD.EQ.0.0) GO TO 5
      FNOLD=VAL
C  NEXT, GET GRADIENT AND NEW SEARCH DIRECTION.
      SUM=0.0
      DO 120 I=1,M
      G(I)=0.0
      IF(TOL(I).LE.0.0) GO TO 120
      X(I)=XOLD(I)+SLASH*TOL(I)
      VAL=FN(X)
      NFN=NFN+1
      X(I)=XOLD(I)
      G(I)=(VAL-FNOLD)/SLASH
120   SUM=SUM+G(I)**2
      SUM=SUM/SUMOLD
      DO 130 I=1,M
      B(I)=-G(I)+SUM*B(I)
130   STEP(I)=B(I)
C
C  SCALE STEP SO EACH ELEMENT IS .LE. 1.0.
      SAVE=0.0
      DO 140 I=1,M
      TEMP=ABS(STEP(I))
      IF(TEMP.GT.SAVE) SAVE=TEMP
140   CONTINUE
      IF(SAVE.NE.0.0) SAVE=1.0/SAVE
C
C  TAKE TRIAL STEP.
      DO 150 I=1,M
      STEP(I)=STEP(I)*TOL(I)*SAVE
C  LOCKUP PARAMETER TENDING TO ZERO.
      IF(STEP(I).GE.0.0.OR.XOLD(I).GT.TOL(I)) GO TO 150
CCCCC TOL(I)=-TOL(I)
CCCCC GO TO 5
150   X(I)=XOLD(I)+STEP(I)
      VAL=FN(X)
      NFN=NFN+1
      IF(VAL.GE.FNOLD) GO TO 910
C  MINIMUM IMPROVED.  DO SEARCH FOR MINIMUM.
      CALL QUAD(FN,M,OLDVAL,VAL,XOLD,STEP,X,NFN)
CCCCC PRINT 97,VAL
97    FORMAT(' NEW VAL=',E20.8)
      GO TO 100
C
C
C  FINISHED.
900   NFN=-NFN
      DO 905  I=1,M
905   TOL(I)=ABS(TOL(I))
      RETURN
910   CONTINUE
      IF(IPASS.GT.5) GO TO 915
```

APPENDIX B

```
C  TRY THROWING OUT A BAD PARAMETER IF IN EARLY STAGES OF MINIMIZATION.
      DO 914 I=1,M
      IF(STEP(I).EQ.0.0) GO TO 914
      SAVE=STEP(I)
      STEP(I)=0.0
      X(I)=XOLD(I)
      VAL=FN(X)
      NFN=NFN+1
      IF(VAL.GE.FNOLD) GO TO 913
      CALL QUAD(FN,M,OLDVAL,VAL,XOLD,STEP,X,NFN)
      B(I)=0.0
      G(I)=0.0
      GO TO 100
913   STEP(I)=SAVE
      X(I)=XOLD(I)+STEP(I)
914   CONTINUE
915   CONTINUE
C  RESTORE X AND VAL.
      VAL=FNOLD
      DO 920 I=1,M
      TOL(I)=ABS(TOL(I))
920   X(I)=XOLD(I)
      RETURN
      END
```

```
      SUBROUTINE QUAD(FN,NPARAM,FNOLD,VAL,XOLD,STEP,X,NFN)
C
C                          -- BY WILLIAM T. WYATT, JR., 1970.
C
C  THIS SUBROUTINE FINDS THE MINIMUM OF THE FUNCTION FN IN THE DIRECTION
C  STEP, GIVEN FNOLD=FN(XOLD), VAL=FN(X), X=XOLD+STEP, AND NPARAM (THE
C  LENGTH OF VECTORS X, XOLD, AND STEP).  A NECESSARY CONDITION IS THAT
C  VAL < FNOLD.  NFN, A COUNTER FOR FUNCTION CALLS, IS INCREMENTED FOR
C  EACH EVALUATION OF FN.  THE SUBROUTINE RETURNS A MINIMUM VAL AND
C  ARGUMENT X SUCH THAT VAL=FN(X), AND STEP SUCH THAT STEP=X-XOLD.
C
C  THE ALGORITHM USES QUADRATIC INTERPOLATION ACCELERATED BY A LOGARITH-
C  MIC BISECTION-TYPE SEARCH.
C
      DIMENSION XOLD(NPARAM),STEP(NPARAM),X(NPARAM)
C  ICOUNT LIMITS THE NUMBER OF FUNCTION EVALUATIONS TO A NUMBER
C  CONVENIENT FOR THIS APPLICATION.  THE USER MAY CHANGE IT.
      ICOUNT=AMAX1(3.0,SQRT(FLOAT(NPARAM)))
      IC=0
      SA=0.
      SB=1.0
      FA=FNOLD
      FB=VAL
C  LOOK FOR A FC.GE.FB.
10    SC=SB*10.0
      DO 20 I=1,NPARAM
      X(I)=XOLD(I)+STEP(I)*SC
20    CONTINUE
      FC=FN(X)
      NFN=NFN+1
      IF(FC.GE.FB) GO TO 100
C  TRY AGAIN.
      FA=FB
      FB=FC
      SA=SB
      SB=SC
      GO TO 10
C  BEGIN MODIFIED QUADRATIC INTERPOLATION FOR MINIMUM.
100   CONTINUE
      IC=IC+1
      IF(IC.GT.ICOUNT) GO TO 170
      TEMP=(SC-SB)/(SB-SA)
      IF(TEMP.GT.4.0) GO TO 110
      IF(TEMP.LT.0.25) GO TO 120
      IF(FA.EQ.FB.OR.FB.EQ.FC) GO TO 170
      CA=((FA-FB)/(SA-SB)-(FB-FC)/(SB-SC))/(SA-SC)
      IF(CA.EQ.0.0) GO TO 110
      CB=(FA-FB)/(SA-SB)-CA*(SA+SB)
      SX=-CB/(2.0*CA)
      GO TO 130
110   CONTINUE
C  EITHER CONVERGING VERY WELL, OR POORLY.  USE LOGARITHMIC SEARCH.
      TEMP=SQRT(TEMP)-1.0
      SX=SB+(SB-SA)*TEMP
      GO TO 130
120   TEMP=SQRT(1.0/TEMP)-1.0
      SX=SB-(SC-SB)*TEMP
130   CONTINUE
      IF(SX.EQ.SB.OR.SX.LE.SA.OR.SX.GE.SC) GO TO 170
```

APPENDIX B

```
C  EVALUATE FUNCTION AT INTERPOLATED POINT.
      DO 135 I=1,MPARAM
      X(I)=XOLD(I)+STEP(I)*SX
135   CONTINUE
      FX=FN(X)
      NFN=NFN+1
      IF(FX.LT.FB) GO TO 150
C  NOT NEW MINIMUM.
      IF(SX.GT.SB) GO TO 140
      SA=SX
      FA=FX
      GO TO 100
140   SC=SX
      FC=FX
      GO TO 100
150   CONTINUE
C  IS NEW MINIMUM.
      IF(SX.LT.SB) GO TO 160
      SA=SB
      FA=FB
      SB=SX
      FB=FX
      GO TO 100
160   SC=SB
      FC=FB
      SB=SX
      FB=FX
      GO TO 100
170   CONTINUE
      VAL=FB
      DO 180 I=1,MPARAM
      STEP(I)=STEP(I)*SB
      X(I)=XOLD(I)+STEP(I)
180   CONTINUE
C  FINISHED.
      RETURN
      END
```

DISTRIBUTION

ADMINISTRATOR
DEFENSE DOCUMENTATION CENTER
ATTN DDC-TCA (12 COPIES)
CAMERON STATION, BUILDING 5
ALEXANDRIA, VA 22314

COMMANDER
US ARMY RSCH & STD GP (EUR)
ATTN LTC JAMES M. KENNEDY, JR.
CHIEF, PHYSICS & MATH BRANCH
FPO NEW YORK 09510

COMMANDER
US ARMY ARMAMENT MATERIEL
READINESS COMMAND
ATTN DRSAR-LEP-L, TECHNICAL LIBRARY
ROCK ISLAND, IL 61299

COMMANDER
US ARMY MISSILE & MUNITIONS
CENTER & SCHOOL
ATTN ATSK-CTD-F
REDSTONE ARSENAL, AL 35809

DIRECTOR
US ARMY MATERIEL SYSTEMS
ANALYSIS ACTIVITY
ATTN DRXSY-MP
ATTN DRXSY-PO
ABERDEEN PROVING GROUND, MD 21005

DIRECTOR
US ARMY BALLISTIC RESEARCH LABORATORY
ATTN DRDAR-TSB-S (STINFO)
ATTN DRXBR-AM, W. VANANTWERP
ATTN DRSTE-EL
ATTN DRDAR-BLE
ABERDEEN PROVING GROUND, MD 21005

U.S. ARMY ELECTRONICS TECHNOLOGY
AND DEVICES LABORATORY
ATTN DELET-DD
FORT MONMOUTH, NJ 07703

TEXAS INSTRUMENTS, INC.
P.O. BOX 226015
ATTN FRANK POBLENZ,
DALLAS, TX 75266

TELEDYNE BROWN ENGINEERING
CUMMINGS RESEARCH PARK
ATTN DR. MELVIN L. PRINCE, MS-44
HUNTSVILLE, AL 35807

ENGINEERING SOCIETIES LIBRARY
345 EAST 47TH STREET
ATTN ACQUISITIONS DEPARTMENT
NEW YORK, NY 10017

DIRECTOR
ARMED FORCES RADIOBIOLOGY RESEARCH
INSTITUTE
DEFENSE NUCLEAR AGENCY
NATIONAL NAVAL MEDICAL CENTER
ATTN RESEARCH PROGRAM COORDINATING
OFFICER
BETHESDA, MD 20014

ASSISTANT TO THE SECRETARY OF DEFENSE
ATOMIC ENERGY
ATTN EXECUTIVE ASSISTANT
WASHINGTON, DC 20301

DIRECTOR
DEFENSE ADVANCED RSCH PROJ AGENCY
ARCHITECT BUILDING
ATTN TIO
1400 WILSON BLVD.
ARLINGTON, VA 22209

DIRECTOR
DEFENSE CIVIL PREPAREDNESS AGENCY
ASSISTANT DIRECTOR FOR RESEARCH
ATTN ADMIN OFFICER
ATTN RE (EO)
ATTN PO (SE)
WASHINGTON, DC 20301

DEFENSE COMMUNICATIONS ENGINEERING
CENTER
ATTN CODE R720, C. STANSBERRY
ATTN CODE R123, TECH LIB
ATTN CODE R400
1860 WIEHLE AVENUE
RESTON, VA 22090

DIRECTOR
DEFENSE COMMUNICATIONS AGENCY
ATTN CCTC C312
ATTN CODE C313
WASHINGTON, DC 20305

DIRECTOR
DEFENSE INTELLIGENCE AGENCY
ATTN RDS-3A
ATTN RDS-3A4, POMPONIO PLAZA
WASHINGTON, DC 20301

DIRECTOR
DEFENSE NUCLEAR AGENCY
ATTN RATN
ATTN DDST
ATTN RAEV
ATTN TITL
ATTN STVL
ATTN VLIS
WASHINGTON, DC 20305

COMMANDER
FIELD COMMAND
DEFENSE NUCLEAR AGENCY
ATTN FCPR
ATTN FCSPM, J. SMITH
ATTN FCLMC
KIRTLAND AFB, NM 87115

DIRECTOR
INTERSERVICE NUCLEAR WEAPONS SCHOOL
ATTN TTV
KIRTLAND AFB, NM 87115

JOINT CHIEFS OF STAFF
ATTN J-3
WASHINGTON, DC 20301

DIRECTOR
JOINT STRATEGIC TARGET PLANNING
STAFF, JCS
OFFUTT AFB
ATTN JSAS
ATTN JPST
ATTN NRI-STINFO LIBRARY
OMAHA, NB 68113

CHIEF
LIVERMORE DIVISION
FIELD COMMAND DNA
DEPARTMENT OF DEFENSE
LAWRENCE LIVERMORE LABORATORY
P.O. BOX 808
ATTN FCPRL
LIVERMORE, CA 94550

NATIONAL COMMUNICATIONS SYSTEM
OFFICE OF THE MANAGER
DEPARTMENT OF DEFENSE
ATTN NCS-TS, CHARLES D. BODSON
WASHINGTON, DC 20305

DIRECTOR
NATIONAL SECURITY AGENCY
DEPARTMENT OF DEFENSE
ATTN R-52, O. VAN GUNTEN
ATTN S232, D. VINCENT
FT. MEADE, MD 20755

UNDER SECY OF DEF FOR RSCH & ENGRG
DEPARTMENT OF DEFENSE
ATTN G. BARSE
ATTN S&SS (OS)
WASHINGTON DC 20301

COMMANDER
BMD SYSTEM COMMAND
DEPARTMENT OF THE ARMY
P.O. BOX 1500
ATTN BMDSC-AOLIB
HUNTSVILLE, AL 35807

COMMANDER
ERADCOM TECHNICAL SUPPORT ACTIVITY
DEPARTMENT OF THE ARMY
ATTN DELCS-K, A COHEN
ATTN DELET-IR, E. HUNTER
FORT MONMOUTH, NJ 07703

COMMANDER
US ARMY ARMOR CENTER
ATTN TECHNICAL LIBRARY
FORT KNOX, KY 40121

COMMANDER
US ARMY COMM-ELEC ENGRG INSTAL
AGENCY
ATTN CCC-PRSO-S
ATTN CCC-CED-SES
FT HUACHUCA, AZ 85613

COMMANDER
US ARMY COMMUNICATIONS COMMAND
COMBAT DEVELOPMENT DIVISION
ATTN ATSI-CD-MD
FT. HUACHUCA, AZ 85613

DISTRIBUTION (Cont'd)

CHIEF
US ARMY COMMUNICATIONS SYS AGENCY
ATTN CCM-RD-T CCM-AD-SV
FORT MONMOUTH, NJ 07703

PROJECT OFFICER
US ARMY COMMUNICATIONS RES &
DEV COMMAND
ATTN DRCPM-ATC
ATTN DRCPM-TDS-BSI
FORT MONMOUTH, NJ 07703

DIVISION ENGINEER
US ARMY ENGINEER DIV HUNTSVILLE
P.O. BOX 1600, WEST STATION
ATTN HNDED-SR
ATTN A. T. BOLT
HUNTSVILLE, AL 35807

US ARMY INTEL THREAT ANALYSIS
DETACHMENT
ROOM 2201, BLDG A
ARLINGTON HALL STATION
ATTN RM 2200, BLDG A
ARLINGTON, VA 22212

COMMANDER
US ARMY INTELLIGENCE & SEC CMD
ARLINGTON HALL STATION
4000 ARLINGTON BLVD
ATTN TECHNICAL LIBRARY
ATTN TECH INFO FAC
ARLINGTON, VA 22212

COMMANDER
US ARMY MISSILE RESEARCH
& DEVELOPMENT COMMAND
ATTN DRCPM-PE-EA, WALLACE O. WAGNER
ATTN DRCPM-PE-EG, WILLIAM B. JOHNSON
ATTN DRDMI-TBD
ATTN DRDMI-EAA
REDSTONE ARSENAL, AL 35809

US ARMY NUCLEAR & CHEMICAL AGENCY
7500 BACKLICK ROAD
BUILDING 2073
ATTN COL A. LOWRY
ATTN DR. J. BERBERET
SPRINGFIELD, VA 22150

COMMANDER
US ARMY TEST AND EVALUATION COMMAND
ATTN DRSTE-FA
ABERDEEN PROVING GROUND, MD 21005

COMMANDER
US ARMY TRAINING AND
DOCTRINE COMMAND
ATTN ATORI-OP-SW
FORT MONROE, VA 23651

COMMANDER
WHITE SANDS MISSILE RANGE
DEPARTMENT OF THE ARMY
ATTN STEWS-TE-AN, J. OKINA
WHITE SANDS MISSILE RANGE, NM 88002

OFFICER-IN-CHARGE
CIVIL ENGINEERING LABORATORY
NAVAL CONSTRUCTION BATTALION CENTER
ATTN CODE L08A (LIBRARY)
ATTN CODE L08A
PORT HUENEME, CA 93041

COMMANDER
NAVAL AIR SYSTEMS COMMAND
ATTN AIR-350F
WASHINGTON, DC 21360

COMMANDER
NAVAL ELECTRONIC SYSTEMS COMMAND
ATTN PME 117-215
WASHINGTON, DC 20360

COMMANDER
NAVAL OCEAN SYSTEMS CENTER
ATTN CODE 015, C. FLETCHER
ATTN RESEARCH LIBRARY
ATTN CODE 7240, S. W. LICHTMAN
SAN DIEGO, CA 92152

COMMANDING OFFICER
NAVAL ORDNANCE STATION
ATTN STANDARDIZATION DIV
INDIAN HEAD, MD 20640

SUPERINTENDENT (CODE 1424)
NAVAL POSTGRADUATE SCHOOL
ATTN CODE 1424
MONTEREY, CA 93940

DIRECTOR
NAVAL RESEARCH LABORATORY
ATTN CODE 4104, EMANUAL L. BRANCATO
ATTN CODE 2627, DORIS R. FOLEN
ATTN CODE 6623, RICHARD L. STATLER
ATTN CODE 6624
WASHINGTON, DC 20375

COMMANDER
NAVAL SHIP ENGINEERING CENTER
DEPARTMENT OF THE NAVY
ATTN CODE 6174D2, EDWARD F. DUFFY
WASHINGTON, DC 20362

COMMANDER
NAVAL SURFACE WEAPONS CENTER
ATTN CODE F32, EDWIN R. RATHBURN
ATTN L. LIBELLO, CODE WR43
ATTN CODE WA51RH, RM 130-108
WHITE OAK, SILVER SPRING, MD 20910

COMMANDER
NAVAL SURFACE WEAPONS CENTER
DAHLGREN LABORAROTY
ATTN CODE DF-56
DAHLGREN, VA 22448

COMMANDER
NAVAL WEAPONS CENTER
ATTN CODE 533, TECH LIB
CHINA LAKE, CA 93555

COMMANDING OFFICER
NAVAL WEAPONS EVALUATION FACILITY
KIRTLAND AIR FORCE BASE
ATTN CODE AT-6
ALBUQUERQUE, NM 87117

OFFICE OF NAVAL RESEARCH
ATTN CODE 427
ARLINGTON, VA 22217

DIRECTOR
STRATEGIC SYSTEMS PROJECT OFFICE
NAVY DEPARTMENT
ATTN NSP-2701, JOHN W. PITSENBERGER
ATTN NSP-2342, RICHARD L. COLEMAN
ATTN NSP-43, TECH LIB
ATTN NSP-27334
ATTN NSP-230, D. GOLD
WASHINGTON, DC 20376

COMMANDER
AERONAUTICAL SYSTEMS DIVISION, AFSC
ATTN ASD-YH-EX
ATTN ENFTV
WRIGHT-PATTERSON AFB, OH 45433

AIR FORCE TECHNICAL APPLICATIONS
CENTER
ATTN TFS, M. SCHNEIDER
PATRICK AFB, FL 32925

AF WEAPONS LABORATORY, AFSC
ATTN NTN
ATTN NT
ATTN EL, CARL E. BAUM,
ATTN ELET
ATTN SUL
ATTN CA
ATTN ELA, J. P. CASTILLO
ATTN ELP
ATTN ELT, W. PAGE
ATTN NES
KIRTLAND AFB, NM 87117

DIRECTOR
AIR UNIVERSITY LIBRARY
DEPARTMENT OF THE AIR FORCE
ATTN AUL-LSE-70-250
MAXWELL AFB, AL 36112

HEADQUARTERS
ELECTRONIC SYSTEMS DEVISION/YSEA
DEPARTMENT OF THE AIR FORCE
ATTN YSEA
HANSCOM AFB, MA 01731

COMMANDER
FOREIGN TECHNOLOGY DIVISION, AFSC
ATTN NICD LIBRARY
ATTN ETDP, B. L. BALLARD
WRIGHT-PATTERSON AFB, OH 45433

COMMANDER
OGDEN ALC/MMEDDE
DEPARTMENT OF THE AIR FORCE
ATTN OO-ALC/MMETH, P. W. BERTHEL
ATTN MMEDO, LEO KIDMAN
ATTN MAJ R. BLACKBURN
HILL AFB, UT 84406

COMMANDER
ROME AIR DEVELOPMENT CENTER AFSC
ATTN TSLD
GRIFFISS AFB, NY 13441

COMMANDER
SACRAMENTO AIR LOGISTICS CENTER
DEPARTMENT OF THE AIR FORCE
ATTN MMCRS, H. A. PELMASTRO
ATTN MMIRA, J. W. DEMES
ATTN MMSRBM, F. R. SPEAR
MCCLELLAN AFB, CA 95652

SAMSO/IN
AIR FORCE SYSTEMS COMMAND
POST OFFICE BOX 92960
WORLDWAY POSTAL CENTER
(INTELLIGENCE)
ATTN IND
LOS ANGELES, CA 90009

SAMSO/MN
AIR FORCE SYSTEMS COMMAND
(MINUTEMAN)
ATTN MNNH, MAJ M. BARAN
ATTN MNNH, CAPT R. I. LAWRENCE
NORTON AFB, CA 92409

SAMSO/YA
AIR FORCE SYSTEMS COMMAND
POST OFFICE BOX 92960
WORLDWAY POSTAL CENTER
ATTN YAPC
LOS ANGELES, CA 90009

STRATEGIC AIR COMMAND/XPFS
ATTN NRI-STINFO LIBRARY
ATTN DEL
ATTN GARNET E. MATZKE
ATTN XPFS, MAJ BRIAN G. STEPHEN
OFFUTT AFB, NB 68113

DEPARTMENT OF ENERGY
ALBUQUERQUE OPERATIONS OFFICE
P.O. BOX 5400
ATTN DOC CON FOR TECH LIBRARY
ATTN OPERATIONAL SAFETY DIV
ALBUQUERQUE, NM 87115

UNIVERSITY OF CALIFORNIA
LAWRENCE LIVERMORE LABORATORY
P.O. BOX 808
ATTN DOC CON FOR TECHNICAL
INFORMATION DEPT
ATTN DOC CON FOR L-06, T. DONICH
ATTN DOC CON FOR L-545, D. MEEKER
ATTN DOC CON FOR L-156, E. MILLER
ATTN DOC CON FOR L-10, H. KRUGER
ATTN DOC CON FOR H. S. CABAYAN
LIVERMORE, CA 94550

LOS ALAMOS SCIENTIFIC LABORATORY
P.O. BOX 1663
ATTN DOC CON FOR BRUCE W. NOEL
ATTN DOC CON FOR CLARENCE BENTON
LOS ALAMOS, NM 87545

SANDIA LABORATORIES
P.O. BOX 5800
ATTN DOC CON FOR C. M. VITTITOE
ATTN DOC CON FOR R. L. PARKER
ATTN DOC CON FOR ELMER F. HARTMAN
ALBUQUERQUE, NM 87115

CENTRAL INTELLIGENCE AGENCY
ATTN RD/SI, RM 5G48, HQ BLDG
FOR OSI/MED/NWB
WASHINGTON, DC 20505

ADMINISTRATOR
DEFENSE ELECTRIC POWER ADMIN
DEPARTMENT OF THE INTERIOR
INTERIOR SOUTH BLDG, 312
ATTN L. O'NEILL
WASHINGTON, DC 20240

DEPARTMENT OF TRANSPORTATION
FEDERAL AVIATION ADMINISTRATION
HEADQUARTERS SEC DIV, ASE-300
800 INDEPENDENCE AVENUE, SW
ATTN SEC DIV ASE-300
WASHINGTON, DC 20591

AEROSPACE CORPORATION
P.O. BOX 92957
ATTN C. B. PEARLSTON
ATTN IRVING M. GARFUNKEL
ATTN JULIAN REINHEIMER
ATTN LIBRARY
ATTN CHARLES GREENHOW
LOS ANGELES, CA 90009

AGBABIAN ASSOCIATES
250 NORTH NASH STREET
ATTN LIBRARY
EL SEGUNDO, CA 90245

AVCO RESEARCH & SYSTEMS GROUP
201 LOWELL STREET
ATTN W. LEPSEVICH
WILMINGTON, MA 01887

BATTELLE MEMORIAL INSTITUTE
505 KING AVENUE
ATTN ROBERT H. BALZEK
ATTN EUGENE R. LEACH
COLUMBUS, OH 43201

BDM CORPORATION
7915 JONES BRANCH DRIVE
ATTN CORPORATE LIBRARY
MCLEAN, VA 22101

BDM CORPORATION
P.O. BOX 9274
ALBUQUERQUE INTERNATIONAL
ATTN LIB
ALBUQUERQUE, NM 87119

BENDIX CORPORATION, THE
RESEARCH LABORATORIES DIVISION
BENDIX CENTER
ATTN MAX FRANK
SOUTHFIELD, MI 48075

BENDIX CORPORATION
NAVIGATION AND CONTROL GROUP
ATTN DEPT 6401
TETERBORO, NJ 07608

BOEING COMPANY
P.O. BOX 3707
ATTN HOWARD W. WICKLEIN
ATTN D. E. ISBELL
ATTN DAVID KEMLE
ATTN B. C. HANRAHAN
ATTN KENT TECH LIB
SEATTLE, WA 98124

BOOZ-ALLEN AND HAMILTON, INC.
106 APPLE STREET
ATTN R. J. CHRISNER
ATTN TECH LIB
TINTON FALLS, NJ 07724

BURROUGHS CORPORATION
FEDERAL AND SPECIAL SYSTEMS GROUP
CENTRAL AVE AND ROUTE 252
P.O. BOX 517
ATTN ANGELO J. MAURIELLO
PAOLI, PA 19301

CALSPAN CORPORATION
P.O. BOX 400
ATTN TECH LIBRARY
BUFFALO, NY 14225

CHARLES STARK DRAPER LABORATORY INC.
555 TECHNOLOGY SQUARE
ATTN KENNETH FERTIG
ATTN TIC MS 74
CAMBRIDGE, MA 02139

CINCINNATI ELECTRONICS CORPORATION
2630 GLENDALE-MILFORD ROAD
ATTN LOIS HAMMOND
CINCINNATI, OH 45241

COMPUTER SCIENCES CORPORATION
6565 ARLINGTON BLVD
ATTN RAMONA BRIGGS
FALLS CHURCH, VA 22046

COMPUTER SCIENCES CORPORATION
1400 SAN MATEO BLVD, SE
ATTN RICHARD H. DICKHAUT
ATTN ALVIN SCHIFF
ALBUQUERQUE, NM 87108

CONTROL DATA CORPORATION
P.O. BOX O
ATTN JACK MEEHAN
MINNEAPOLIS, MN 55440

CUTLER-HAMMER, INC.
AIL DIVISION
COMAC ROAD
ATTN EDWARD KARPEN
DEER PARK, NY 11729

DIKEWOOD INDUSTRIES, INC
1009 BRANDBURY DRIVE, SE
ATTN TECH LIB
ATTN L. WAYNE DAVIS
ALBUQUERQUE, NM 87106

DISTRIBUTION (Cont'd)

DIKEWOOD INDUSTRIES, INC.
1100 GLENDON AVENUE
ATTN K. LER
LOS ANGELES, CA 90024

E-SYSTEMS, INC
GREENVILLE DIVISION
P.O. BOX 1056
ATTN JOLETA MOORE
GREENVILLE, TX 75401

EFFECTS TECHNOLOGY, INC.
5383 HOLLISTER AVENUE
ATTN S. CLOW
SANTA BARBARA, CA 93111

EG&G WASHINGTON ANALYTICAL
SERVICES CENTER, INC.
P.O. BOX 10218
ATTN C. GILES
ALBUQUERQUE, NM 87114

EXXON NUCLEAR COMPANY, INC.
RESEARCH AND TECHNOLOGY CENTER
2955 GEORGE WASHINGTON WAY
ATTN DR, A. W. TRIVELPIECE
RICHLAND, WA 99352

FAIRCHILD CAMERA AND INSTRUMENT CORP
464 ELLIS STREET
ATTN SEC CON FOR DAVID K. MYERS
MOUNTAIN VIEW, CA 94040

FORD AEROSPACE & COMMUNICATIONS CORP
3939 FABIAN WAY
ATTN TECHNICAL LIBRARY
PALO ALTO, CA 94303

FORD AEROSPACE & COMMUNICATIONS
OPERATIONS
FORD & JAMBOREE ROADS
ATTN KEN C. ATTINGER
ATTN E. R. PONCELET, JR.
NEWPORT BEACH, CA 92663

FRANKLIN INSTITUTE, THE
20TH STREET AND PARKWAY
ATTN RAMIE H. THOMPSON
PHILADELPHIA, PA 19103

GENERAL DYNAMICS CORP
ELECTRONICS DIVISION
P.O. BOX 81125
ATTN RSCH LIB
SAN DIEGO, CA 92138

GENERAL DYNAMICS CORPORATION
INTER-DIVISION RESEARCH LIBRARY
KEARNY MESA
P.O. BOX 80847
ATTN RESEARCH LIBRARY
SAN DIEGO, CA 98123

GENERAL ELECTRIC CO.-TEMPO
CENTER FOR ADVANCED STUDIES
816 STATE STREET (PO DRAWER QQ)
ATTN DASIAC
ATTN ROYDEN R. RUTHERFORD
ATTN WILLIAM MCNAMERA
SANTA BARBARA, CA 93102

GENERAL ELECTRIC COMPANY
AEROSPACE ELECTRONICS SYSTEMS
FRENCH ROAD
ATTN CHARLES M. HEWISON
UTICA, NY 13503

GENERAL ELECTRIC COMPANY
P.O. BOX 5000
ATTN TECH LIB
BINGHAMTON, NY 13902

GENERAL ELECTRIC CO.-TEMPO
ALEXANDRIA OFFICE
HUNTINGTON BUILDING, SUITE 300
2560 HUNTINGTON AVENUE
ATTN DASIAC
ALEXANDRIA, VA 22303

GENERAL RESEARCH CORPORATION
SANTA BARBARA
P.O. BOX 6770
ATTN TECH INFO OFFICE
SANTA BARBARA, CA 93111

GEORGIA INSTITUTE OF TECHNOLOGY
GEORGIA TECH RESEARCH INSTITUTE
ATTN R. CURRY
ATLANTA, GA 30332

GEORGIA INSTITUTE OF TECHNOLOGY
OFFICE OF CONTRACT ADMINISTRATION
ATTN RES & SEC COORD FOR HUGH DENNY
ATLANTA, GA 30332

GRUMMAN AEROSPACE CORPORATION
SOUTH OYSTER BAY ROAD
ATTN L-01 35
BETHPAGE, NY 11714

GTE SYLVANIA INC.
ELECTRONICS SYSTEMS GRP-EASTERN DIV
77 A STREET
ATTN CHARLES A. THORNHILL, LIBRARIAN
ATTN LEONDARD L. BLAISDELL
NEEDHAM, MA 02194

GTE SYLVANIA, INC.
189 B STREET
ATTN CHARLES H. RAMSBOTTOM
ATTN DAVID D. FLOOD
ATTN EMIL P. MOTCHOK
ATTN H & V GROUP, MARIO A. NUREFORA
ATTN J. WALDRON
NEEDHAM HEIGHTS, MA 02194

HARRIS CORPORATION
HARRIS SEMICONDUCTOR DIVISION
P.O. BOX 883
ATTN V PRES & MGR PRGMS DIV
MELBOURNE, FL 32901

HAZELTINE CORPORATION
PULASKI ROAD
ATTN TECH INFO CTR, M. WAITE
GREENLAWN, NY 11740

HONEYWELL INCORPORATED
AVIONICS DIVISION
2600 RIDGEWAY PARKWAY
ATTN S&RC LIB
ATTN RONALD R. JOHNSON
MINNEAPOLIS, MN 55413

HONEYWELL INCORPORATED
AVIONICS DIVISION
13350 U.S. HIGHWAY 19 NORTH
ATTN M.S 725-5, STACEY H. GRAFF
ATTN W. E STEWART
ST. PETERSBURG, FL 33733

HUGHES AIRCRAFT COMPANY
CENTINELA AND TEALE
ATTN JOHN B. SINGLETARY
ATTN CTDC 6/E110
ATTN KENNETH R. WALKER
CULVER CITY, CA 90230

IIT RESEARCH INSTITUTE
ELECTROMAG COMPATABILITY ANAL CTR
NORTH SEVERN
ATTN ACOAT
ANNAPOLIS, MD 21402

IIT RESEARCH INSTITUTE
10 WEST 35TH STREET
ATTN IRVING N. MINDEL
ATTN JACK E. BRIDGES
CHICAGO, IL 60616

INSTITUTE FOR DEFENSE ANALYSES
400 ARMY-NAVY DRIVE
ATTN TECH INFO SERVICES
ARLINGTON, VA 22202

INTL TEL & TELEGRAPH CORPORATION
500 WASHINGTON AVENUE
ATTN TECHNICAL LIBRARY
ATTN ALEXANDER T. RICHARDSON
NUTLEY, NJ 07110

IRT CORPORATION
P.O. BOX 81087
ATTN C. B. WILLIAMS
ATTN DENNIS SWIFT
SAN DIEGO, CA 92138

JAYCOR
SANTA BARBARA FACILITY
P.O. BOX 2008
ATTN W. A. RADASKY
SANTA BARBARA, CA 93120

JAYCOR
1401 CAMINO DEL MAR
ATTN ERIC P. WENAAS
ATTN RALPH H. STARL
DEL MAR, CA 92014

JAYCOR
205 S WHITING STREET, SUITE 500
ATTN LIB
ALEXANDRIA, VA 22304

DISTRIBUTION (Cont'd)

KAMAN SCIENCES CORPORATION
1500 GARDEN OF THE GODS ROAD
ATTN ALBERT P. BRIDGES
ATTN W. FOSTER RICH
ATTN WALTER E. WARE
ATTN FRANK H. SHELTON
ATTN JERRY I. LUBELL
ATTN PHIL TRACY
ATTN WERNER STARK
COLORADO SPRINGS, CO 80907

LITTON SYSTEMS, INC.
DATA SYSTEMS DIVISION
8000 WOODLEY AVENUE
ATTN EMC GP
ATTN M848-61
VAN NUYS, CA 91409

LITTON SYSTEMS, INC.
AMECOM DIVISION
5115 CALVERT ROAD
ATTN J. SKAGGS
COLLEGE PARK, MD 20740

LOCKHEED MISSLES AND SPACE
COMPANY, INC
P.O. BOX 504
ATTN L. ROSSI
ATTN SAMUEL I. TAIMUTY
ATTN H. E. THAYN
ATTN GEORGE F. HEATH
ATTN BENJAMIN T. KIMURA
SUNNYVALE, CA 94086

LOCKHEED MISSILES AND SPACE
COMPANY, INC.
3251 HANOVER STREET
ATTN TECH INFO CTR D/COLL
PALO ALTO, CA 94304

M.I.T. LINCOLN LABORATORY
P.O. BOX 73
ATTN LEONA LOUGHLIN
LEXINGTON, MA 02173

MARTIN MARIETTA CORPORATION
ORLANDO DIVISION
P.O. BOX 5837
ATTN MONA C. GRIFFITH
ORLANDO, FL 32805

MCDONNEL DOUGLAS CORPORATION
POST OFFICE BOX 516
ATTN TOM ENDER
ST. LOUIS, MO 63166

MCDONNELL DOUGLAS CORPORATION
5301 BOLSA AVENUE
ATTN STANLEY SCHNEIDER
ATTN TECH LIBRARY SERVICES
HUNTINGTON BEACH, CA 92647

MISSION RESEARCH CORPORATION
P.O. DRAWER 719
ATTN EMP GROUP
ATTN WILLIAM C. HART
ATTN C. LONGMIRE
SANTA BARBARA, CA 93102

MISSION RESEARCH CORPORATION
EM SYSTEM APPLICATIONS DIVISION
1400 SAN MATEO BLVD, SE, SUITE A
ATTN DAVID E. MERIWETHER
ATTN L. N. MCCORMICK
ALBUQUERQUE, NM 87108

MISSION RESEARCH CORPORATION
-SAN DIEGO
P.O. BOX 1209
ATTN V. A. J. VAN LINT
LA JOLLA, CA 92038

MITRE CORPORATION, THE
P.O. BOX 208
ATTN M. F. FITZGERALD
BEDFORD, MA 01730

NORDEN SYSTEMS, INC.
HELEN STREET
ATTN TECHNICAL LIBRARY
NORWALK, CT 06856

NORTHROP RESEARCH TECHNOLOGY CENTER
ONE RESEARCH PARK
ATTN LIBRARY
PALOS VERDES PENN, CA 90274

NORTHROP CORPORTION
ELECTRONIC DIVISION
2301 WEST 120TH STREET
ATTN LEW SMITH
ATTN RAD EFFECTS GRP
HAWTHORNE, CA 90250

PHYSICS INTERNATIONAL COMPANY
2700 MERCED STREET
ATTN DOC CON
SAN LEANDRO, CA 94577

R.&.D ASSOCIATED
P.O. BOX 9695
ATTN S. CLAY ROGERS
ATTN RICHARD R. SCHAEFER
ATTN DOC CON
ATTN M. GROVER
ATTN C. MACDONALD
MARINA DEL REY, CA 90291

R&D ASSOCIATES
1401 WILSON BLVD
SUITE 500
ATTN J. BOMBARDT
ARLINGTON, VA 22209

RAND CORPORATION
1700 MAIN STREET
ATTN LIB-D
ATTN W. SOLLFREY
SANTA MONICA, CA 90406

RAYTHEON COMPANY
HARTWELL ROAD
ATTN GAJANAN H. JOSI
BEDFORD, MA 01730

RAYTHEON COMPANY
528 BOSTON POST ROAD
ATTN HAROLD L. FLESCHER
SUDBURY, MA 01776

RCA CORPORATION
GOVERNMENT SYSTEMS DIVISION
ASTRO ELECTRONICS
P.O. BOX 800, LOCUST CORNER
EAST WINDSOR TOWNSHIP
PRINCETON, NJ 08540

RCA CORPORATION
DAVID SARNOFF RESEARCH CENTER
P.O. BOX 432
ATTN SECURITY DEPT, L. MINICH
PRINCETON, NJ 08540

RCA CORPORATION
CAMDEN COMPLEX
FRONT & COOPER STREETS
ATTN OLIVE WHITEHEAD
ATTN R. W. TOSTROM
CAMDEN, NJ 08012

ROCKWELL INTERNATIONAL CORPORATION
P.O. BOX 3105
ATTN N. J. RUDIE
ATTN J. L. MONROE
ATTN V. J. MICHEL
ATTN D/243-068, 031-CA31
ANAHEIM, CA 92803

ROCKWELL INTERNATIONAL CORPORATION
SPACE DIVISION
12214 SOUTH LAKEWOOD BOULEVARD
ATTN B. E. WHITE
DOWNEY, CA 90241

ROCKWELL INTERNATIONAL CORPORATION
815 LAPAHM STREET
ATTN E-1, DIV TIC (BACB)
EL SEGUNDO, CA 90245

ROCKWELL INTERNATIONAL CORPORATION
P.O. BOX 369
ATTN F. A. SHAW
CLEARFIELD, UT 84015

SANDERS ASSOCIATES, INC.
95 CANAL STREET
ATTN 1-6270, R. G. DESPATHY, SR P E
NASHUA, NH 03060

SCIENCE APPLICATIONS, INC.
P.O. BOX 277
ATTN FREDERICK M. TESCHE
BERKELEY, CA 94701

SCIENCE APPLICATIONS, INC.
P.O. BOX 2351
ATTN R. PARKINSON
LA JOLLA, CA 92038

SCIENCE APPLICATIONS, INC.
HUNTSVILLE DIVISION
2109 W. CLINTON AVENUE
SUITE 700
ATTN NOEL R. BYRN
HUNTSVILLE, AL 35805

SCIENCE APPLICATIONS, INC.
8400 WESTPARK DRIVE
ATTN WILLIAM L. CHADSEY
MCLEAN, VA 22101

DISTRIBUTION (Cont'd)

SINGER COMPANY
ATTN: SECURITY MANAGER
FOR TECH INFO CTR
1150 MC BRIDE AVENUE
LITTLE FALLS, NJ 07424

SPERRY RAND CORPORATION
SPERRY MICROWAVE ELECTRONICS
P.O. BOX 4648
ATTN MARGARET CORT
CLEARWATER, FL 33518

SPERRY RAND CORPORATION
SPERRY DIVISION
MARCUS AVENUE
ATTN TECH LIB
GREAT NECK, NY 11020

SPERRY RAND CORPORATION
SPERRY FLIGHT SYSTEMS
P.O. BOX 21111
ATTN D. ANDREW SCHOW
PHOENIX, AZ 85036

SPIRE CORPORATION
P.O. BOX D
ATTN JOHN R. UGLUM
ATTN ROGER G. LITTLE
BEDFORD, MA 01730

SRI INTERNATIONAL
333 RAVENSWOOD AVENUE
ATTN ARTHUR LEE WHITSON
MENLO PARK, CA 94025

SYSTEMS, SCIENCE AND SOFTWARE, INC.
P.O. BOX 1620
ATTN ANDREW R. WILSON
LA JOLLA, CA 92038

TEXAS INSTRUMENTS, INC.
P.O. BOX 6015
ATTN TECH LIB
ATTN DONALD J. MANUS
DALLAS, TX 75265

TRW DEFENSE & SPACE SYS GROUP
ONE SPACE PARK
ATTN O. E. ADAMS
ATTN R. K. PLEBUCH
ATTN L. R. MAGNOLIA
ATTN H. H. HOLLOWAY
ATTN W. GRAGARO
REDONDO BEACH, CA 90278

TEXAS TECH UNIVERSITY
P.O. BOX 5404 NORTH COLLEGE STATION
ATTN TRAVIS L. SIMPSON
LUBBOCK, TX 79417

UNITED TECHNOLOGIES CORP
HAMILTON STANDARD DIVISION
BRADLEY INTERNATIONAL AIRPORT
ATTN CHIEF ELEC DESIGN
WINDSOR LOCKS, CT 06069

WESTINGHOUSE ELECTRIC CORPORATION
ADVANCED ENERGY SYSTEMS DIV
P.O. BOX 10864
ATTN TECH LIB
PITTSBURGH, PA 15236

US ARMY ELECTRONICS RESEARCH
& DEVELOPMENT COMMAND
ATTN TECHNICAL DIRECTOR, DRDEL-CT

HARRY DIAMOND LABORATORIES
ATTN CO/TD/TSO/DIVISION DIRECTORS
ATTN RECORD COPY, 81200
ATTN HDL LIBRARY 81100 (3 COPIES)
ATTN HDL LIBRARY (WOODBRIDGE) 81100
ATTN TECHNICAL REPORTS BRANCH, 81300
ATTN CHAIRMAN, EDITORIAL COMMITTEE
ATTN CHIEF, 21000
ATTN CHIEF, 22000
ATTN CHIEF, 22100 (3 COPIES)
ATTN CHIEF, 22300
ATTN CHIEF, 22800
ATTN CHIEF, 22900
ATTN CHIEF, 13300
ATTN CHIEF, 21100 (3 COPIES)
ATTN CHIEF, 21200
ATTN CHIEF, 21300 (5 COPIES)
ATTN CHIEF, 21400 (2 COPIES)
ATTN CHIEF, 21500
ATTN BALICKI, F. W., 20240
ATTN WIMENITZ, F. N., 20240
ATTN TALLERICO, A., 47400
ATTN BIXBY, R., 22900
ATTN WYATT, W. T., 21300 (20 COPIES)